J Theor Appl Phys (2016) 10:163–193
DOI 10.1007/s40094-016-0214-z

RESEARCH

High-pressure and temperature-induced structural, elastic, and thermodynamical properties of strontium chalcogenides

Dinesh Varshney[1] · S. Jain[1,2] · S. Shriya[1] · R. Khenata[3]

Received: 29 September 2015 / Accepted: 22 March 2016 / Published online: 16 April 2016

Abstract Pressure- and temperature-dependent mechanical, elastic, and thermodynamical properties of rock salt to CsCl structures in semiconducting SrX (X = O, S, Se, and Te) chalcogenides are presented based on model interatomic interaction potential with emphasis on charge transfer interactions, covalency effect, and zero point energy effects apart from long-range Coulomb, short-range overlap repulsion extended and van der Waals interactions. The developed potential with non-central forces validates the Cauchy discrepancy among elastic constants. The volume collapse (V_P/V_0) in terms of compressions in SrX at higher pressure indicates the mechanical stiffening of lattice. The expansion of SrX lattice is inferred from steep increase in V_T/V_0 and is attributed to thermal softening of SrX lattice. We also present the results for the temperature-dependent behaviors of hardness, heat capacity, and thermal expansion coefficient. From the Pugh's ratio ($\phi = B_T/G_H$), the Poisson's ratio (v) and the Cauchy's pressure (C_{12}–C_{44}), we classify SrO as ductile but SrS, SrSe, and SrTe are brittle material. To our knowledge these are the first quantitative theoretical prediction of the pressure and temperature dependence of mechanical stiffening, thermally softening, and brittle nature of SrX (X = O, S, Se, and Te) and still await experimental confirmations.

Keywords Chalcogenides · High pressure · Elastic properties · Mechanical properties · Thermal expansion

Introduction

Strontium chalcogenides SrX (X = O, S, Se, and Te) witnesses a pressure-induced phase transition from the six folds coordinated rock salt structure ($B1$) to the eightfold coordinated CsCl structure ($B2$) [1]. Strontium chalcogenides SrX (X = O, S, Se, and Te) have wide range of scientific and technological application in television picture tube glass, catalysis, microelectronics, luminescent devices, radiation dosimetry, fast high resolution optically stimulated luminescent devices, and infrared sensitive device [2].

Many theoretical investigations concerning transition pressure, volume collapse, higher order elastic constants, bulk modulus have been investigated using quantum mechanical calculations. The full-potential linear augmented plane-wave method (FP-LAPW) has been exercised to probe the ground state properties such as lattice parameter, bulk modulus, and its pressure derivative, elastic constant and structural stability of the compound SrS, SrSe, and SrTe, respectively [1–12].

The Burger mechanism was used to study lattice dynamics of SrX (X = S, Se and Te) and their pressure dependence in both $B1$ and $B2$ phases to predict the temperature and pressure dependence of thermal expansion coefficient, bulk modulus, and the heat capacity [2]. The Energy-dispersive X-ray diffraction (EDXD) observes the transition pressure (P_T) in SrO = 36 GPa [3, 4], SrS = 18

✉ Dinesh Varshney
vdinesh33@rediffmail.com

[1] Materials Science Laboratory, School of Physics, Vigyan Bhavan, Devi Ahilya University, Khandwa Road Campus, Indore 452001, India

[2] Department of Physics, S. D. Bansal College of Engineering, Indore 453331, India

[3] Laboratoire de Physique Quantique et de Modélisation Mathématique (LPQ3 M), Département de Technologie, Université de Mascara, 29000 Mascara, Algeria

GPa [3, 7], SrSe = 14 GPa [3], and SrTe = 12 GPa, respectively [3, 5]. A percentage volume collapse at P_T in going from ($B1$ to $B2$) of about 13.0 in SrO [3, 4], 11.4 in SrS [3, 7], 10.7 in SrSe [3], and 11.1 in SrTe [3, 5] is reported using high-pressure X-rays diffraction studies. The elastic stiffness constant is obtained using ultrasonic pulse-echo technique [6].

Structural properties of the $B1$ and $B2$ phases of alkaline earth oxides and their phase transition have been investigated using ab initio linear muffin-tin-orbital (LMTO) method [9]. The phase transition of SrS from NaCl ($B1$) structure to CsCl ($B2$) structure is investigated by means of ab initio plane-wave pseudo potential density function theory [10]. The Born–Mayer potential-based calculations also predict the phase-transition pressure, bulk modulus, first-order pressure derivatives of bulk modulus in SrX (X = S, S, Se, and Te) [11]. The elastic properties and their pressure dependence of $B1$-type alkaline earth oxides are calculated using the ab initio full-potential linear muffin-tin-orbital (FP-LMTO) [12].

In view of the reported literature on technological important monochalcogenides as SrX (X = O, S, Se, and Te) [1–12], we notice that both the quantum calculations and the lattice model calculations predict the pressure-induced ground state properties and no efforts have been made to explore the temperature-dependent elastic, thermal, and thermodynamical properties of these chalcogenides. In view of these, we made systematic efforts to investigate (a) pressure-induced, and (b) temperature-induced properties. We further made efforts to compare them by means of thermodynamical variables as pressure and temperature. We further note that we properly incorporate the (a) the charge transfer interactions, (b) the covalency effect, and (c) the zero point energy effects in the model Hamiltonian.

For SrX (X = O, S, Se, and Te), although structural transitions are known to some extent, but to the best of our knowledge, no systematic efforts have been made to explore the high-pressure and high-temperature dependence of the aggregate elastic constants, their anisotropy, Melting temperature, Poisson's ratio, elastic wave velocity, Grüneisen parameter, isothermal (adiabatic) compressibility, Shear (Young's) modulus, Hardness, Lamé's constant, Kleinman parameter, and thermodynamic properties as Debye temperature, heat capacity and thermal expansion coefficient either in rock salt or CsCl structures.

The method

The understanding of pressure-dependent structural properties as first-order structural phase transition, associated volume collapse; elastic properties as ductility, mechanical stiffening, thermal softening, anisotropy in elastic constants, Shear (Young's) modulus, hardness, Lame's constant, Kleinman's parameter, shear and longitudinal elastic wave velocity as well thermodynamics properties viz Debye temperature, melting temperature, heat capacity and thermal expansion coefficient of SrX needs the formulation of an effective interatomic potential. The idea we have in mind follows: the change in force constants is small, the short-range interactions are effective up to the second-neighbor ions, and the atoms are held together with harmonic elastic forces without any internal strains within the crystal. Usually, the applications of pressures cause an increase in the overlap of adjacent ions in a crystal and hence, charge transfer takes place between the overlapping electron shells. The transferred charges interact with all others of the lattice via Coulomb's law and give rise to charge transfer interactions under pressure. We have also incorporated zero point energy effect, although it has a small effect in Gibbs free energy.

An isolated phase is stable only when it's free energy is minimized for the specified thermodynamic conditions. As the temperature or pressure or any other variable acting on the systems is altered, the free energy changes smoothly and continuously. A phase transition is said to occur when the changes in structural details of the phase are caused by such variations of free energy. The SrX ceramic transforms from their initial $B1$ to $B2$ structure under pressure. The stability of a particular structure is decided by the minima of Gibbs's free energy, $G = U + PV - TS$, U is internal energy, which at 0 K corresponds to the cohesive energy, S is the vibrational entropy at absolute temperature T, pressure P, and volume V.

We must mention that the calculations presented here assume zero temperature, i.e., the frozen ionic degrees of freedom. Although, the experimental results are obtained at ambient temperature inferring a certain small temperature dependence of the transition pressures in the range of low temperatures as well on polycrystalline or bulk samples. It is worth considering the lattice calculation results as representative of the results that would be obtained under the actual experimental conditions. At zero temperature, the thermodynamically stable phase at a given pressure P is the one with lowest entropy, and the thermo dynamical potential is the Helmholtz free energy (H).

The Gibbs's free energies for NaCl ($B1$) and CsCl ($B2$) phase is given by Born equation $G_{B1}(r) = U_{B1}(r) + 2Pr^3$ for NaCl ($B1$) and $G_{B2}(r') = U_{B2}(r') + 1.54Pr'^3$ for CsCl ($B2$) phase become equal at the phase-transition pressure P and at zero temperature, i.e., $G_{B1} = G_{B2}$ [13]. Here, the abbreviation U_{B1} (r) to the Rock Salt ($B1$) and U_{B2} (r') stands for the CsCl ($B2$) phase. Here, V_{B1} (=$2r^3$) and V_{B2} (=$1.54r'^3$) as the unit cell volume and are being the nearest

neighbor distance for $B1$ (NaCl) and $B2$ (CsCl) phase, and its relevant expressions are

$$U_{B1} = (-\alpha_M Ze^2/r)[Z + 2nf(r)] - Cr^{-6} - Dr^{-8} + nb\beta_{ij}\exp\left[\left(r_i + r_j - r_{ij}\right)/\rho\right] + (n'b/2)\left[\beta_{ii}\exp\left(\left(2r_i - kr_{ij}\right)/\rho\right) + \beta_{jj}\exp\left(\left(2r_j - kr_{ij}\right)/\rho\right)\right] + \left[\{\hbar < \omega^2 >^{1/2}/2\right] \quad (1)$$

$$U_{B2} = (-\alpha_M^{'} Ze^2/r')[Z + 2mf(r')] - Cr'^{-6} - Dr'^{-8} + mb\beta_{ij}\exp\left[\left(r_i + r_j - r_{ij}^{'}\right)/\rho\right] + (m'b/2)\left[\beta_{ii}\exp\left(\left(2r_i - k'r_{ii}^{'}\right)/\rho\right) + \beta_{jj}\exp\left(\left(2r_j - k'r_{jj}^{'}\right)/\rho\right)\right] + \left[\{\hbar < \omega^2 >^{1/2}/2\}\right] \quad (2)$$

Due to complex nature of bonds in SrX (X = O, S, Se, and Te,) the ionic charge for Sr and X atom cannot be determined uniquely. The calculations of the Madelung energy are thus modified by incorporating the covalency effects [14–17]. The charge in above equations is thus written incorporating the polarization of a spherical shaped dielectric in displacing the constituent positive ions. The charge transfer interactions caused by the deformation of the electron shells of the overlapping ions and the covalency effects are the major attributes of long-range Coulomb effects. The IIA–VIA semiconducting compound contains covalent bonds so that some electrons are distributed over the region between neighboring atoms; in such situation energies due to charge dipole–dipole and charge dipole–quadruple interaction. The induced charge dipole–dipole and charge dipole–quadruple (van der Waals) interaction are the third and fourth terms, which are the short-range vdW attractive potential energies.

The fifth and sixth terms are short-range (SR) repulsive energy due to the overlap repulsion between ij, ii and jj ions. α_m (α_m') are the Madelung constants for $B1$ ($B2$) phases. β_{ij} are the Pauling coefficient defined as $\beta_{ij} = 1 + (Z_i/n_i) + (Z_j/n_j)$ with $Z_i(Z_j)$ and $n_i(n_j)$ as the valence and the number of electrons in the outermost orbit. The number of the nearest neighbors for unlike are n (=6) and for like n' (=6) in case of $B1$ (NaCl). Similarly, numbers of the nearest neighbors for unlike m (=8) and m' (=3) are for $B2$ (CsCl). The Ze is the ionic charge, k (k') is being the structure factor for $B1$ ($B2$) structures, and b (ρ) is the hardness (range) parameters. The nearest neighbor ion separations for $B1$ ($B2$) structures are being r (r'), respectively.

The last term is the lowest possible energy of the system and is due to the zero point energy. Here, $\langle\omega^2\rangle^{1/2}$ ($=k_B\theta_D/\hbar$) is the mean square frequency related to the Debye temperature θ_D. The Debye temperature can be known either from Heat capacity measurements or from the Bulk modulus value using $\theta_D = (\hbar/k_B)\sqrt{(5r_0B_T/\mu)}$. Herein, r_0, B, and μ are the equilibrium distance, Bulk modulus, and reduced mass of the compounds. Henceforth, model potential for ground state incorporates the attractive, repulsive, and zero point energy.

We use the variational approach to deduce the overall vdW coefficients C (charge dipole–dipole) and D (charge dipole–quadruple) [18]. The short-range vdW coefficients due to induced charge dipole–dipole and charge dipole–quadruple interactions caused by Sr atom and X atom are

$$c_{ij} = \frac{3}{2}\frac{e\hbar}{\sqrt{m_e}}\alpha_i\alpha_j\left[\left(\frac{\alpha_i}{N_i}\right)^{1/2} + \left(\frac{\alpha_j}{N_j}\right)^{1/2}\right]^{-1}, \quad (3)$$

$$d_{ij} = \frac{27}{8}\frac{\hbar^2}{m_e}\alpha_i\alpha_j\left[\left(\frac{\alpha_i}{N_i}\right)^{1/2} + \left(\frac{\alpha_j}{N_j}\right)^{1/2}\right]^2 \times\left[\left(\frac{\alpha_i}{N_i}\right) + \frac{20}{3}\left(\frac{\alpha_i\alpha_j}{N_iN_j}\right)^{1/2} + \left(\frac{\alpha_j}{N_j}\right)\right]^{-1}. \quad (4)$$

$$c_{ii} = \frac{3}{2}\frac{e\hbar}{\sqrt{m_e}}\alpha_i\alpha_i\left[\left(\frac{\alpha_i}{N_i}\right)^{1/2} + \left(\frac{\alpha_i}{N_i}\right)^{1/2}\right]^{-1}, \quad (5)$$

$$d_{ii} = \frac{27}{8}\frac{\hbar^2}{m_e}\alpha_i\alpha_i\left[\left(\frac{\alpha_i}{N_i}\right)^{1/2} + \left(\frac{\alpha_i}{N_i}\right)^{1/2}\right]^2 \times\left[\left(\frac{\alpha_i}{N_i}\right) + \frac{20}{3}\left(\frac{\alpha_i\alpha_i}{N_iN_i}\right)^{1/2} + \left(\frac{\alpha_i}{N_i}\right)\right]^{-1} \quad (6)$$

$$c_{jj} = \frac{3}{2}\frac{e\hbar}{\sqrt{m_e}}\alpha_j\alpha_j\left[\left(\frac{\alpha_j}{N_j}\right)^{1/2} + \left(\frac{\alpha_j}{N_j}\right)^{1/2}\right]^{-1}, \quad (7)$$

$$d_{jj} = \frac{27}{8}\frac{\hbar^2}{m_e}\alpha_j\alpha_j\left[\left(\frac{\alpha_j}{N_j}\right)^{1/2} + \left(\frac{\alpha_j}{N_j}\right)^{1/2}\right]^2 \times\left[\left(\frac{\alpha_j}{N_j}\right) + \frac{20}{3}\left(\frac{\alpha_j\alpha_j}{N_jN_j}\right)^{1/2} + \left(\frac{\alpha_j}{N_j}\right)\right]^{-1}. \quad (8)$$

In the above equations, the notations: m_e, e, and Z are mass of the electron, charge, and valence of the constituent metallic element, respectively. The symbols α_i and α_j represents the polarizabilities of ith and jth ion, respectively. The effective numbers of electrons responsible for polarization are symbolized by N_i and N_j. The lattice sums S_{ij}, and T_{ij} enable one to compute the overall vdW coefficients C and D in terms of c and d values determined from Eqs. 1 to 8. The lattice sums S_{ij}, and T_{ij} are expressed as [19]:

$$C = c_{ij}S_{ij} + c_{ii}S_{ii} + c_{jj}S_{jj} \quad (9)$$

$$D = d_{ij}T_{ij} + d_{ii}T_{ii} + d_{jj}T_{jj}. \quad (10)$$

The binary alloy as SrX is a tetrahedrally coordinated covalent material and the complex chemical bonding corroborate both ionic and covalent nature. The Coulomb interaction between ions of Sr and *X* atoms leads to charge transfer interactions. Apart this, the covalent character of bond bending and stretching also needs to be incorporated in the potential. Thus, the second term in Eqs. (1, 2) is an algebraic sum of non-central many-body forces as the charge transfer force parameter and the force parameter arises due to covalent nature, i.e., $f(r) = f_{\mathrm{cti}} + f_{\mathrm{cov}}$. The charge transfer between ions of Si and C atoms is denoted in terms of a force parameter f_{cti} and is expressed as [20–22]:

$$f_{\mathrm{cti}} = f_0 \exp(-r/\rho) \tag{11}$$

Here, r_i (r_j) is the ionic radii of $i(j)$ ion.

The complex chemical bonding in II–VI semiconducting compounds infers SrX as partially ionic and partially covalent in bonding. The attractive forces due to covalent nature thus modifies the charge and is now the effective charge. The polarization effects originate from changes in covalency due to Sr–Sr, Sr–*X*, and *X*–*X* interacting electric fields. The covalency term in the interaction potential is thus expressed as [16, 17]:

$$f_{\mathrm{cov}}(r) = \frac{4e^2 V_{sp\sigma}^2}{r_0 E_{\mathrm{g}}^3} \tag{12}$$

Here, $V_{sp\sigma}$ represents the transfer matrix element between the outermost *p* orbital and the lowest excited of *s* state. The transfer energy of electron from *p* to the *s* orbital is denoted as E_{g}. The effective charge e_{S}^* of SrX is related with the number of electrons transferred to the unoccupied orbital's from its surrounding nearest neighbor. The electron density is thus $n_{\mathrm{c}} = 1 - e_{\mathrm{S}}^*/e$. Thus in Sr*X* for overlap distortion effect $e_{\mathrm{S}}^* \neq e$. The transfer matrix element $V_{sp\sigma}$ and the transfer energy E_{g} is related to electron density as $n_{\mathrm{c}}/12 \cong V_{sp\sigma}^2/E_{\mathrm{g}}^2$. The effective charge e_{S}^* is thus

$$\frac{V_{sp\sigma}^2}{E_{\mathrm{g}}^2} = \frac{1 - e_s^*}{12} \tag{13}$$

The transfer energy E_{g} is

$$E_{\mathrm{g}} = E - I + (2\alpha - 1)\frac{e^2}{r} \tag{14}$$

Here, *E* is the electron affinity for C and *I* is the ionization potential of constituent atom.

The Szigeti effective charge e_{S}^* $(=Ze)^*$ is written in terms of the optical static dielectric constant ε_0 and the high frequency dielectric constant ε_∞ as [23–31]:

$$e_{\mathrm{s}}^{*2} = \frac{9\mu\omega_{\mathrm{TO}}^2(\varepsilon_0 - \varepsilon_\infty)}{4\pi N_{\mathrm{k}}(\varepsilon_\infty + 2)^2} \tag{15}$$

and

$$\frac{e_{\mathrm{s}}^{*2}}{e^2} = \frac{9V\mu\omega_{\mathrm{TO}}^2(\varepsilon_0 - \varepsilon_\infty)}{4\pi e^2(\varepsilon_\infty + 2)^2} \tag{16}$$

The symbol μ is the reduced mass, N_{k} is the number of atoms present per unit cell volume, i.e., $N_{\mathrm{k}} = 1/V$, ω_{TO} is the long wavelength transverse optical phonon frequency. Thus, for Sr*X* e_{S}^* deviates from *e* and is attributed to covalent nature of Sr–Sr, Sr–*X*, and *X*–*X* bonds.

Usually material documents a transition when the thermo dynamical potential relevant to the given ensemble of the lower pressure phase equals that for some other structure in the absence of any barrier. The low-pressure phase becomes the stable phase above this coexistence pressure. After determining the stable phase we also compute the higher order elastic constants, their pressure derivatives and anisotropy. With these understanding of interatomic potential in Sr*X*, we have four material parameters, namely, modified ionic charge; hardness, range, force parameter [Z_{m}, *b*, ρ, $f(r)$]. Values of them can be deduced from equilibrium conditions [32–37].

Results and discussion

The application of pressure, temperature and magnetic field probably transform materials from one structure to another. The relative stability of two crystal structures requires an extremely accurate prediction. The interatomic interaction potential with charge transfer interactions caused by ions of Sr and X atom and covalent nature of Sr–Sr, Sr–*X*, and *X*–*X* bonds are effective in studying the structural phase transitions and elastic properties of tetrahedrally coordinated semiconductors Sr*X*. We evaluate the phase-transition pressure by computing the Gibbs free energy $G = U + PV - TS$ for the rock salt and cesium chloride phases. We note that the Gibbs free energy is thus the enthalpy H $(=U + PV)$ at $T = 0$ K.

While doing high-pressure experiments, the huge applied pressure causes a reduction of the material volume. The temperature variations during the experiments will normally produce much smaller changes in the relative stabilities of different phases. Thus, the Gibbs free energy at zero temperature, which is the enthalpy *H* is measured. The thermodynamically stable phase of crystal at 0 K and at ambient pressure *P* is the one with the lowest enthalpy. Thus, the zero temperature theoretical calculations are valid with experiment. In a situation when temperature variations are large during experiment for certain materials the effects of finite temperature may be significant. With these assumptions, we investigate structural and elastic properties of SrX in an ordered way.

The thermo dynamical potential G or H in SrX is computed involving modified ionic charge, hardness, range, and charge transfer parameters [Z_m, b, ρ, $f(r)$] as [23–31]:

$$\left|\frac{dU(r)}{dr}\right|_{r=r_0} = 0 \tag{17}$$

Also, the bulk modulus (B_T):

$$\left|\frac{d^2U(r)}{dr^2}\right|_{r=r_0} = (9kr_0)^{-1}B_T \tag{18}$$

We first deduce vdW coefficients C and D involved in expressions (1) and (2) from the Slater-Kirkwood variational method [18], for SrX material parameters, and are enlisted in Table 1. The charge dipole–dipole and charge dipole–quadruple vdW coefficients are influenced by electronic polarizabilities. The polarizability values have been obtained from least-squares fit of experimental refraction data using additive rule and a Lorentz factor of $4\pi/3$ [38, 39]. We consider that the SrX to be partially ionic and covalent to discuss their structural, mechanical, elastic, and thermo dynamical properties in a systematic manner.

As a next step, we use the experimental data on lattice constant (a) [3, 5–7, 40] the bulk modulus (B_T) [3], ionic (Ze), effective charge (e_s^*), and the second-order aggregate elastic constant C_{12} (C_{44}) [6, 8] for determining the material parameters. The computed strontium SrX (X = O, S, Se, and Te) chalcogenides, material parameter of hardness (b), range (ρ), and non-central many-body forces arose due to charge transfer (f_{cti}) and covalency (f_{cov}) for SrX is illustrated in Table 1. The effective charge e_S^* depends on the values of optical dielectric constant ε_s and the high-frequency dielectric constant ε_∞. The value of long wave length transverse optical phonon frequency ω_{TO} is taken from [2] to have the effective charge e_S^* and hence the covalency contribution.

We then minimize the Gibbs's free energies $G_{B1}(r)$ and $G_{B2}(r')$ for the equilibrium interatomic spacing (r) and (r') to determine structural phase transition of SrX (X = O, S, Se, and Te). Table 1 shows the optimized values of equilibrium interatomic spacing in $B1$ and $B2$ phases. The Gibbs's free energy $G_{B1}(r)$ [$G_{B2}(r')$] as functions of pressure (P) for SrX is discerned in Fig. 1a. At zero pressure, the Gibb's free energy for $B1$ crystal phase is more negative therefore; it is thermodynamically and mechanically

Table 1 Estimated and input crystal data: vdW coefficients [c_{ii}, c_{ij}, c_{jj}, C, d_{ii}, d_{ij}, d_{jj}, D], lattice constant (a_0), bulk modulus (B_T), second-order elastic constant C_{12} (C_{44}), optimized value of ionic radii r_i (r_j), hardness (b), range (ρ), charge transfer parameter $f(r)$, equilibrium distance (r_0), Gibb's free energy $G_{B1}(r)$; $G_{B2}(r')$, and cohesive energy for SrX (X = O, S, Se, and Te) in $B1$ phase at zero pressure

S. no.	Input parameters	SrO	SrS	SrSe	SrTe
1	c_{ii} (10^{-60} erg cm^6)	28.266	28.266	28.266	28.266
2	c_{ij} (10^{-60} erg cm^6)	52.249	95.1	108.314	132.858
3	c_{jj} (10^{-60} erg cm^6)	100.997	384.424	520.886	847.487
4	C (10^{-60} erg cm^6)	461.363	1000	1210	1667
5	d_{ii} (10^{-76} erg cm^8)	13.958	13.958	13.958	13.958
6	d_{ij} (10^{-76} erg cm^8)	33.409	87.421	109.342	156.948
7	d_{jj} (10^{-79} erg cm^8)	76.245	453.118	679.393	1300
8	D (10^{-76} erg cm^8)	241.406	724.114	949.36	1490
9	a_0 (Å)	5.160 [6]	6.024 [7]	6.234 [3]	6.659 [5]
10	B_T (GPa)	91 [3]	58 [3]	45 [3]	40 [3]
11	C_{12} (GPa)	45 [6]	17.5 [8]	13.4 [8]	7.8 [8]
12	C_{44} (GPa)	56 [6]	62.5 [8]	53.7 [8]	44.8 [8]
13	r_i (Å)	1.01	1.01	1.01	1.01
14	r_j (Å)	1.37	1.37	1.40	1.44.2.11
15	b (10^{-12} erg)	1.64	5.469	6.227	9.063
16	ρ (10^{-9} cm)	2.66	3.12	3.54	3.71
17	$f(r)$ (10^{-3})	0.6261	1.303	5.026	5.495
18	Equilibrium distance (Å) r_0 ($B1$)	2.67	3.11	3.26	3.46
19	Equilibrium distance (Å) r_0' ($B2$)	2.8	3.25	3.43	3.64
20	Gibb's free energy (kJ/mol) G_{B1} (r)	−1122	−1196	−1759	−1305
21	Gibb's free energy (kJ/mol) G_{B2} (r')	−1123	−1197	−1716	−1035
22	Cohesive energy (eV)	−33.93, −32.91 [11]	−60.70, −28.79 [11]	−61.43, −27.42 [11]	−67.26 −26.10 [11]

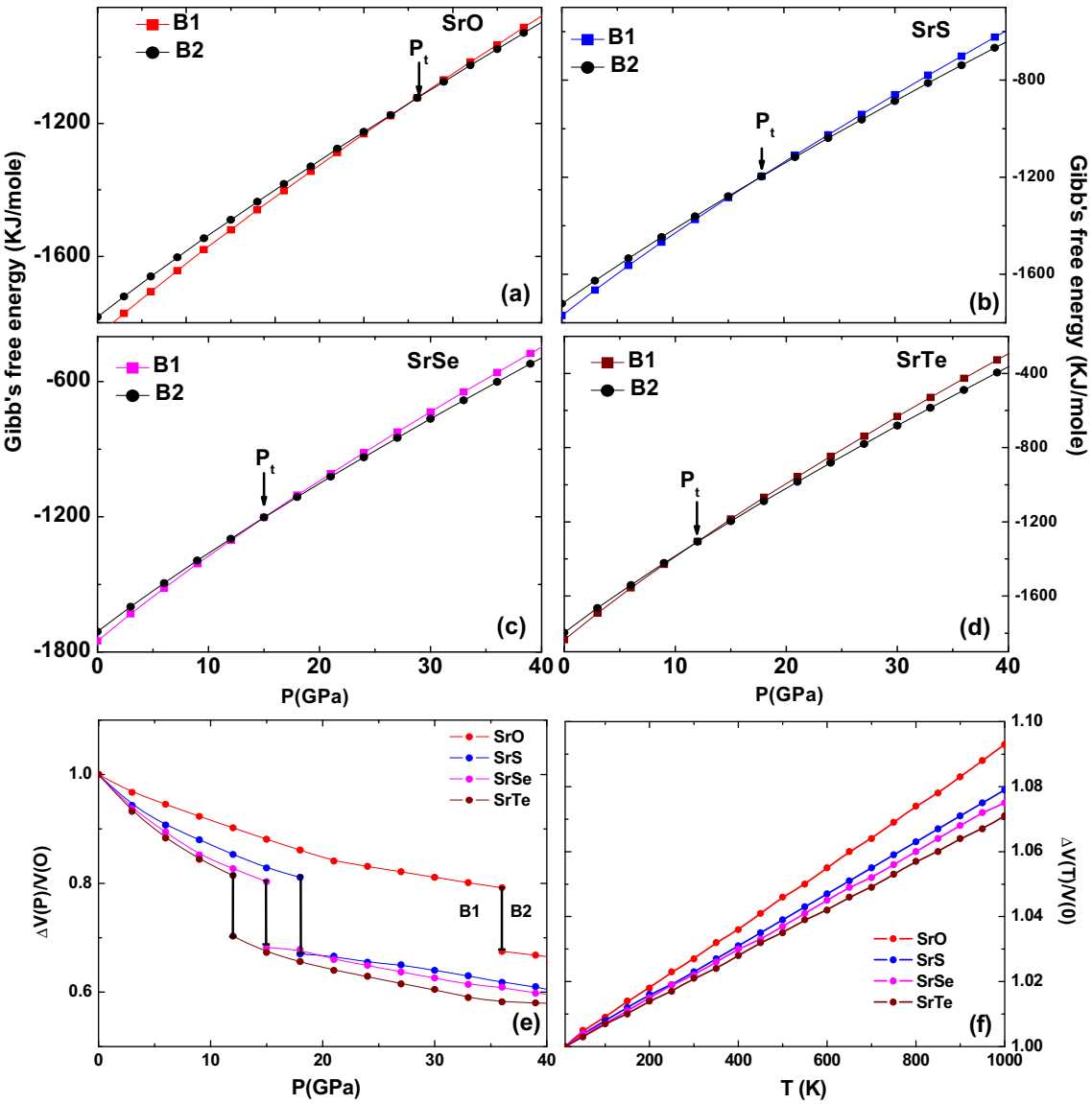

Fig. 1 Variation of Gibb's free energy for *B1* and *B2* phases with pressure and normalized volume with pressure and temperature

stable, while the *B*2 is not. On the other hand, above the phase-transition pressure (P_T), the Gibb's free energy for *B*1 system becomes more negative than *B*2 phase, implying *B*1 phase will be more stable. With the above-deduced material parameters, we have computed the cohesive energy for Sr*X* (*X* = O, S, Se, and Te), which is consistent with earlier deduced value [11].

Sr*X* shows a crystallographic transition from *B*1 to *B*2 in certain pressure range. Table 2 illustrates the computed phase-transition pressure (P_T) and compared with available experimental data [3–5] and theoretical results [1, 2, 11]. P_T for Sr*X* (*X* = O, S, Se, and Te) is consistent with the experimental and other reported values and is attributed to proper formulation of interatomic potential, which considers the various interactions explicitly the non-central many-body forces as charge transfer interactions and covalency effects, as well as use of materials parameter based on experimental data. We may comment that any computational technique has its own limitations related to the chosen materials basic parameters, basic sets, as well the accuracy and precisions used apart from the approximations laid in the method. Needless to suggest that there is always a variation in estimated parameters by each technique.

The values of relative volumes associated with various compressions are estimated from [41]

$$\frac{V_P}{V_0} = \left(1 + \frac{B'}{B_0}P\right)^{-1/B'}, \tag{19}$$

Here, V_0 (B_0) is the cell volume (bulk modulus) of Sr*X* at ambient conditions and V_P is at finite pressure. The symbol

Table 2 Calculated transition pressure (P_T), volume collapse (%), aggregate second-order elastic constants (C_{11}, C_{12} and C_{44}), aggregate bulk modulus (B_T), tetragonal moduli (C_S), pressure derivatives of SOECs (dB_T/dP, dC_{44}/dP and dC_S/dP), anisotropy parameter (γ_i^2), Cauchy discrepancy (Δ_1^2), isotropic shear modulus (G_H), Voigt's shear modulus (G_V), Reuss's shear modulus (G_R), Young's modulus (E), Poisson ratio (v), Grüneisen parameter (γ_G) for SrX (X = O, S, Se, and Te) in *B1* phase at zero pressure

S. no.	Property		Present	Expt.	Others
1	Transition pressure P_T (GPa)	SrO	35.5	36.0 [3, 4]	30.9–35.3 [1, 11]
		SrS	17.6	18.0 [3]	16.7–17.7 [1, 2]
		SrSe	14.9	14.0 [3]	13.6–16.2 [1, 2]
		SrTe	11.92	12.0 [3, 5]	12.3–14.1 [1, 2]
2	Volume collapse (%)	SrO	11.7	13.0 [3, 4]	11.8 [9]
		SrS	14.1	11.4 [3]	11.5 [2]
		SrSe	12.1	10.7 [3]	10.5 [2]
		SrTe	11.1	11.1 [3, 5]	9.50 [2]
3	C_{11} (GPa)	SrO	133.6		170 [12]
		SrS	79.7		113.9 [10]
		SrSe	57.3		
		SrTe	54.8		
4	C_{12} (GPa)	SrO	34.05		48 [12]
		SrS	17.81		19.4 [10]
		SrSe	14.74		
		SrTe	13.0		
5	C_{44} (GPa)	SrO	46.8		59 [12]
		SrS	26.6		30.3 [10]
		SrSe	23.9		
		SrTe	21.0		
6	B_T (GPa)	SrO	67.3	88 [6]	86–106 [1, 12]
		SrS	38.4		53.9–58.6 [1, 10]
		SrSe	28.9		50.3 [1]
		SrTe	26.9		39.7 [1]
7	C_S (GPa)	SrO	49.8		
		SrS	30.9		
		SrSe	21.3		
		SrTe	20.9		
8	dB_T/dP	SrO	5.40	6.0 [6]	4.08–4.5 [9, 12]
		SrS	5.35		4.19–4.66 [8, 10]
		SrSe	4.92		3.76 [8]
		SrTe	4.94	5.00 [5]	3.23 [8]
9	dC_{44}/dP	SrO	0.266	−0.2 [6]	
		SrS	0.111		
		SrSe	0.104		
		SrTe	4.53		
10	dC_S/dP	SrO	4.87	4.0 [6]	
		SrS	5.05		
		SrSe	4.40		
		SrTe	4.53		
11	$\gamma_1^2(10^{10}\ Nm^{-2})$	SrO	0.063		
		SrS	0.163		
		SrSe	−0.108		
		SrTe	0.005		
12	$\Delta_1^2\ (10^{10}\ Nm^{-2})$	SrO	−1.276		
		SrS	−0.088		
		SrSe	−0.091		
		SrTe	−0.781		

Table 2 continued

S. no.	Property		Present	Expt.	Others
13	G_H (10^{10} Nm^{-2})	SrO	4.8		
		SrS	2.82		
		SrSe	2.28		
		SrTe	2.08		
14	G_V (10^{10} Nm^{-2})	SrO	4.8		
		SrS	2.83		
		SrSe	2.28		
		SrTe	2.08		
15	G_R (10^{10} Nm^{-2})	SrO	4.8		
		SrS	2.82		
		SrSe	2.28		
		SrTe	2.08		
16	E ($10^{10}Nm^{-2}$)	SrO	11.63		
		SrS	6.81		
		SrSe	5.42		
		SrTe	4.97		
17	v	SrO	0.212		
		SrS	0.205		
		SrSe	0.188		
		SrTe	0.192		
18	γ_G	SrO	1.523		
		SrS	1.508		
		SrSe	1.403		
		SrTe	1.425		

B' is the pressure derivative of the bulk modulus. Figure 1e documents the estimated value of pressure-dependent radius for both $B1$ and $B2$ structures, the curve of volume collapse (V_P/V_0) with pressure to show phase diagram for SrX. The phase diagram will let us estimate the magnitude of the discontinuity in volume at the transition pressure. The value of relative volumes is shown in Table 2. It is also compared with various experimental [3–5] and other theoretical works [2, 9]. Compressions in SrX at higher pressure indicate the mechanical stiffenening of lattice.

Figure 1f discerns the variation of V_T/V_0 as functions of temperature in $B1$ phase. Here, V_T symbolizes the volume at various temperatures and V_0 at zero temperature and zero pressure volumes, respectively. A steep increase in the ratio V_T/V_0 with increasing temperature infers expansion of SrX lattice and is susceptible to temperature. On the other hand, SrX is compressed at higher pressures as showed in Fig. 1e. SrX lattice is thus thermally softened and mechanical stiffened. The normalized volume V_T/V_0 dependences on temperature is not known for SrX, but the present behavior is consistent with available experimental [42] and theoretical [43] data on Li_2O.

The response of any material that undergoes stress, deforms and then recovers and returns to its original shape after stress ceases leads to the determination of elastic properties. The elastic properties are vital in generating information about the binding characteristic between adjacent atomic planes, anisotropic character of binding and structural stability. Apart from the structural stability of SrX in NaCl ($B1$) and CsCl ($B2$) structures, we now compute the aggregate elastic constants at normal and under hydrostatic pressure. Deduced values are documented in Table 2.

Using the stress–strain coefficients, one determines the second-order aggregate elastic constants C_{ij} under hydrostatic pressure with respect to finite strain. Also, proper parameterization of long-range as Coulomb and non-central many-body forces as charge transfer interactions and covalency effect, short-range as overlap repulsion extended up to the second-neighbor ions, van der Waals interactions and zero point energy effects are differentially needed.

The cubical symmetry of SrX dealt with three independent elastic constants C_{ij}. C_{11} is a response of resistance to deformation by a stress applied on (1,0,0) plane with polarization in the direction $\langle 100 \rangle$. C_{11} probes elasticity in length and a longitudinal strain produces a change in C_{11}. C_{44} refers to the measurement of resistance to deformation with respect to a shearing stress applied across the (100) plane with polarization in the $\langle 010 \rangle$ direction. C_{12} and C_{44} are related to the elasticity in shape, which is a shear

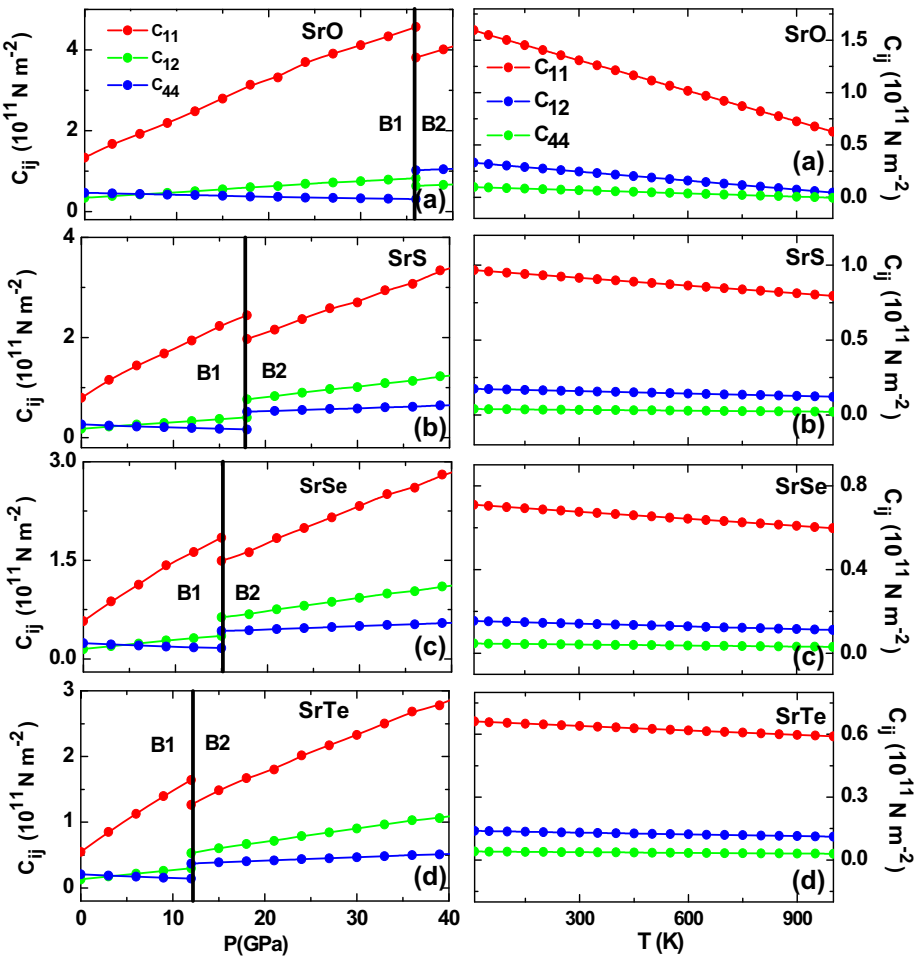

Fig. 2 Variation of aggregate second-order elastic constants (C_{ij}) with pressure and temperature

constant. A transverse strain causes a change in shape without a change in volume and hence C_{12} and C_{44} are less sensitive of pressure as compared to C_{11}.

The variation of three independent second-order aggregate elastic constants (SOECs): C_{11}, C_{12}, and C_{44} with external pressure for SrX in $B1$ and $B2$ phase is first discussed. It is as seen from Fig. 2a that C_{11} and C_{12} increases with increase in pressure in both $B1$ and $B2$ phases. Also, C_{44} decreases with the increase of pressure away from zero till the phase-transition pressures and then increases in $B1$ phase. Similar observations have earlier been reported in SrX [10, 12]. A crossover of C_{12} and C_{44} in CaS has also been reported [44]. At phase-transition pressures, SrX has witnessed a discontinuity in aggregate second-order elastic constants C_{ij}, which identifies the first-order phase transition. Thus, the proposed interaction potential incorporating charge transfer interactions ions of Sr and X atom and covalency effects caused by Sr–Sr, Sr–X, and X–X bonds consistently explains the high-pressure elastic behavior.

The variations in C_{ij} with temperatures (T) for SrX are plotted in Fig. 2b. It can be seen that the aggregate elastic constants C_{ij} (T) decreases linearly with the temperature in rock salt phase. We note that the pressure dependence of aggregate elastic constants C_{ij} (P) documents an increasing trend (please see Fig. 2a). The physical interpretation of temperature dependence of C_{ij} showed that (a) values of C_{11} decreases more steeply with enhancing temperature, (b) C_{12}, and C_{44}, are less sensitive to temperature for SrX, (c) C_{11} is remarkably larger than C_{12}, and C_{44}, and (d) values of all aggregate elastic constants C_{ij} are influenced by temperature dependence indicating that anharmonicity is substantial. Deduced values of C_{ij} with temperatures (T) are documented in Table 4. As far as we know, there are no experimental results available for comparison. From the second-order aggregate elastic constants pressure and temperature-dependent behavior, we comment that SrX lattice is mechanical stiffened and thermally softened.

Born criterion for a lattice to be mechanically stable infers that the elastic energy density must be a positive definite quadratic function of strain. The principal minors (alternatively the Eigen values) of the elastic constant matrix should all be positive at ambient conditions. The

mechanical stability conditions for a crystal suggest that elastic constants of a cubic crystal follow [13],

$$B_T = (C_{11} + 2C_{12})/3 > 0, \quad (20)$$

$$C_{11}, C_{44} > 0, \quad (21)$$

and

$$C_S = (C_{11} - C_{12})/2 > 0. \quad (22)$$

Here, C_{ij} are conventional aggregate elastic constants and B_T is bulk modulus. We represent, C_{44} and C_S as the shear and tetragonal moduli of a cubic crystal.

Table 2 illustrates the computed values of bulk modulus (B_T), shear moduli (C_{44}), and tetragonal moduli (C_S) which validates the elastic stability criteria for SrX in $B1$ phase. The second-order elastic constants critically depend upon pressure leading to $C_{12}-C_{44} \neq 0$. The mechanically stable phases for cubic crystal satisfy the Born criteria: $C_{12}-C_{44} > 0$. The equilibrium condition leads to $B_1 + B_2 = -1.261Z_m^2$ with emphasis on charge transfer interactions as well covalency effects. For optimized values of r_i (r_j) the Cauchy discrepancy: $C_{12}-C_{44}$ is nonzero at zero pressure and at zero temperature. It is also valid when the many-body non-central forces are not involved in long-range forces. The short-range and long-range effects are naturally of similar order of magnitude. This is due to the fact C_{ij} are calculated at optimized values of equilibrium distances rather than at experimental values.

Table 2 illustrates the calculated values of pressure derivatives of aggregate second-order elastic constants (dB_T/dP, dC_{44}/dP, and dC_S/dP). These are compared with available experimental [5, 6] and theoretical studies [8–10, 12]. For mechanical stability the shear elastic constant C_{44} is nonzero and is known by combining mechanical stability with minimum energy conditions. The high-pressure stability also suggests that the stable phase of the crystal posses the lowest potential energy among the mechanically stable lattices [45].

The elasticity in SrX is thus probed by a non-central many-body force potential, which assumes that the interatomic forces have a certain shape and directionality. The Cauchy discrepancy is defined as $\Delta_1^2 = C_{12}-C_{44}-2P$. Here, Δ_1^2 is a measure of the contribution from the non-central many-body force. However, for pure central interatomic potentials, Cauchy relation is $C_{12} = C_{44} + 2P$.

At zero pressure, the Cauchy discrepancy (Δ_1^2) in Strontium chalcogenides is about -1.276 (SrO), -0.088 (SrS), -0.091 (SrSe), -0.781×10^{10} (SrTe) Nm^{-2}. The Δ_1^2 further enhances on increasing the pressure in both phases as depicted from Fig. 3a. In SrX, larger deviation of Δ_1^2 essentially points to the importance of the many-body non-central (charge transfer and covalency) interaction in the interatomic potential and anharmonic effects are substantial at high pressures. The strength of non-central many-body forces incorporating charge transfer interactions and covalency effects is witnessed by significant deviation in Δ_1^2 at different pressures not only in Rock salt but also in cesium chloride structure, although weak. The importance of many-body non-central forces and anharmonic effects are further explored by analyzing the higher order elastic constants explicitly the third-order elastic constants. Usually, the anharmonic effects are noticeable at high pressure as reflected from elastic constants behavior.

The anisotropy in second-order elastic constants is reflected from geophysical activities of various materials and alloys. The anisotropic parameter γ is unity for isotropic elasticity. As far as cubic crystal is concerned although it is isotropic in structure, but has elastic anisotropy other than unity. This is a consequence of fourth rank tensor property of elasticity.

We define elastic anisotropic parameter γ_1^2 in terms of aggregate C_{ij} as [46]:

$$\gamma_1^2 = \frac{C_{11} - C_{12} - 2C_{44}}{2C_{44}} \quad (23)$$

The pressure dependence of the elastic anisotropic parameter γ_1^2 in SrX is shown in Fig. 3b. It is evident that γ_1^2 increases with advancement of pressure below transition pressure in $B1$ phase of SrX. It is insensitive to pressure in $B2$ phase. A jump has been noted at P_T inferring first-order structural phase transition. The value of anisotropic parameter γ_1^2 for SrX is given in Table 2 at $T = 0$ K and $P = 0$ GPa.

During mechanical processing, explicitly in fabrication the melting ranges of materials and alloys are substantial. The usage of an alloy in the applications as the success of the melting and casting operations depends on the correct selection of temperature. Once solidified and primary processed (rolling or forging), the melting temperature has little significance to designers, engineers and users. The melting temperature influence elevated temperature properties, such as creep strength, the researchers have limited interest. The pressure dependence of the melting temperature: $T_M = 553K + 5.91C_{11}K/\text{GPa}$ for SrX in $B1$ and $B2$ phase is discerned in Fig. 4a. It is noticed that T_M enhances with increased pressure or in other words the resistance to deformation by a stress increases. The value of melting temperature T_M for SrX is given in Table 3 at $T = 0$ K and $P = 0$ GPa An increase in T_M with variations in pressure infers the hardening or stiffening of the lattice. Higher melting temperature symbolizes higher shear modulus (G), and Young's modulus (E) values that we shall see later on. The data on its melting under high pressure are very limited and extremely contradictory, which does not allow one to make any conclusions about congruent or incongruent

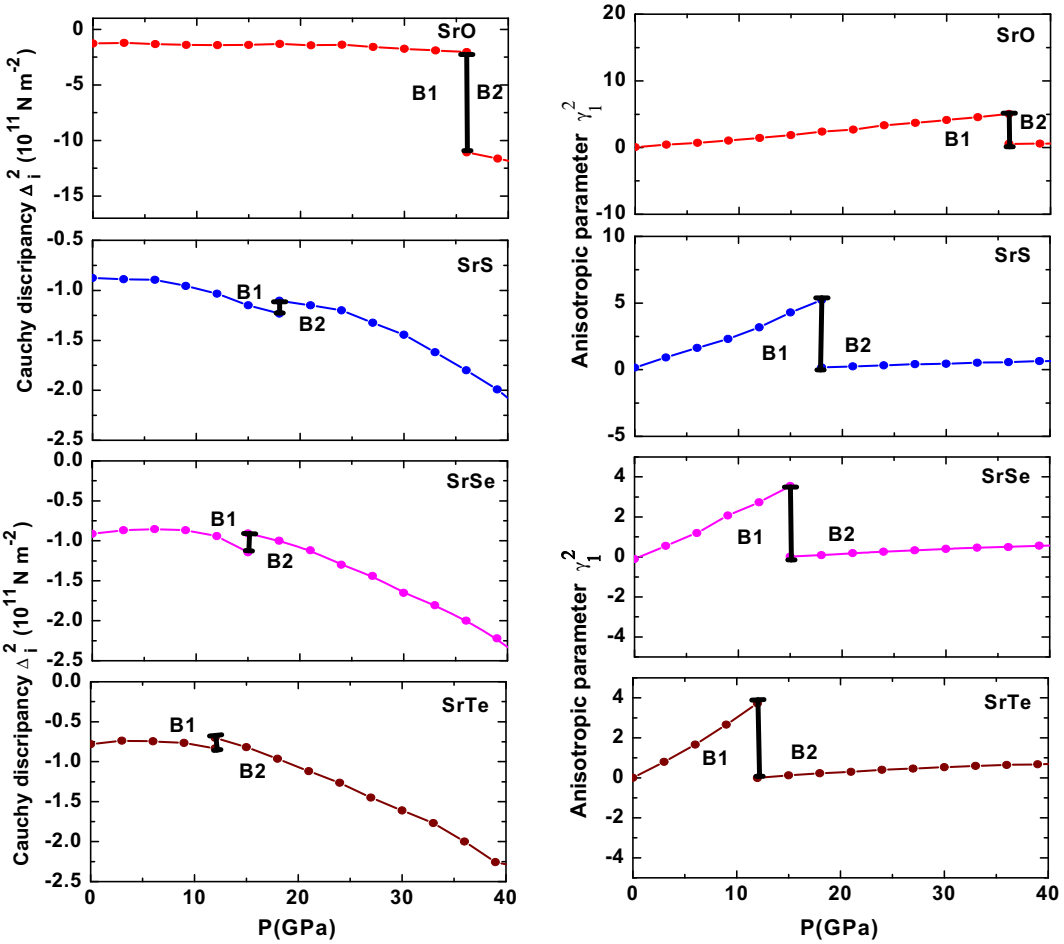

Fig. 3 Variation of Cauchy discrepancy (Δ_1^2) and elastic anisotropy (γ_1^2) in second-order elastic constant (C_{ij}) with pressure and temperature

melting behavior as well the slope of the melting curve of Sr*X*.

Figure 4b shows the temperature dependence of the melting temperature for Sr*X* estimated from the C_{11} elastic constant as discussed previously. At room temperature its value is about 1327 K (SrO), 1094 K (SrS), 952 K (SrSe), 931 K (SrTe) in *B*1 phase. The suppressed T_M with increased temperature indicates that there is a decrease in the resistance to deformation by a stress induced due to temperature. The suppressed T_M infers the weakening of the lattice as a result of thermal softening.

For cubic lattice, three second-order elastic constants and the six non-vanishing third-order elastic constants are obtained from crystal geometry. The anharmonicity of a crystal lattice is successfully probed in terms of higher order elastic constants. The third-order terms in the strain variables are deduced from derivatives of elastic energy (please see Appendix for both rock salt *B*1 and cesium chloride *B*2 phases). For Sr*X* the third-order aggregate elastic constants: C_{111}, C_{112}, C_{166} are negative and C_{123}, C_{144}, C_{456} are positive at $P = 0$ GPa, i.e., in *B*1 phase. We note that no such efforts have been made in the past for third-order elastic constants of Sr*X*. Thus, deduced information on pressure-dependent C_{ijk} will serve as a guideline for future research and its application in materials technology. This information is useful, as the structural strengths of a material are successfully known from the knowledge of elastic constants. The microstructures developed on the applied pressure and temperature can be known from third-order elastic constants variations.

The variation of aggregate third-order elastic constants (TOECs) with pressure for Sr*X* in *B*1 and *B*2 phase is sketched in Fig. 5. For Sr*X* only C_{456} increase with enhancing pressure. Other TOEC's as C_{111}, C_{112}, C_{166} infers a decreasing trend and C_{123}, C_{144} are insensitive with enhancing pressure. Furthermore, aggregate elastic constants C_{ijk} inferring the anharmonic effects are influenced by application of pressure in Sr*X*. In the present interatomic potential, C_{ijk} are affected by the inclusion of second-nearest-neighbor interaction and are influenced by the short-range interactions. Also, many-body non-central forces as long-range Coulomb, charge transfer interactions

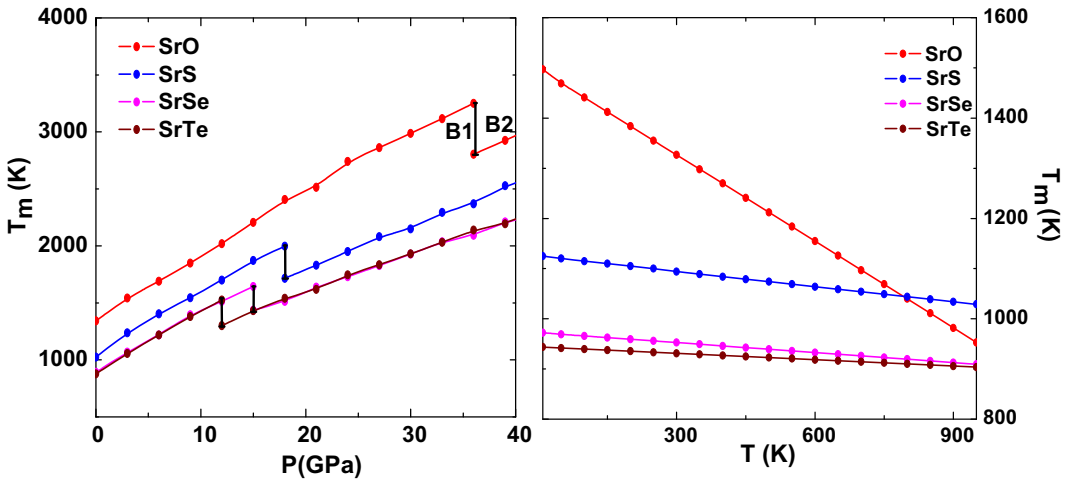

Fig. 4 Variation of melting temperature (T_M) with pressure and temperature

Table 3 Calculated aggregate third-order elastic constant (C_{ijk}), third-order elastic constant anisotropy parameter (γ_i^3), First and second Lame's constant (λ, μ), longitudinal (v_l), shear (v_s) and average elastic wave velocity (v_m), Kleinman parameter (ξ) thermodynamical properties: force constant (f), Reststrahlen frequency (v_0), compressibility (β), average elastic constant (C_s), Debye temperature (θ_D), melting temperature (T_M), force constant (f), hardness (H_v), of SrX (X = O, S, Se, and Te) in *B1* phase at zero pressure

S. no.	Elastic properties	SrO	SrS	SrSe	SrTe
1	C_{111} (10^{10} Nm^{-2})	−252.70	−150.40	−100.70	−95.64
2	C_{112} (10^{10} Nm^{-2})	−17.85	−9.20	−6.99	−6.06
3	C_{123} (10^{10} Nm^{-2})	67.9	40.1	30.5	2.69
4	C_{144} (10^{10} Nm^{-2})	69.0	41.5	34.7	3.08
5	C_{166} (10^{10} Nm^{-2})	−19.78	−10.79	−10.07	−8.86
6	C_{456} (10^{10} Nm^{-2})	6.38	3.84	3.40	3.05
7	γ_1^3	−17.445	−15.711	−23.479	−22.286
8	γ_2^3	−2.784	−2.593	−2.447	−2.42
9	γ_3^3	3.093	−2.947	−2.991	−2.957
10	λ (10^{10} Nm^{-2})	3.53	1.96	1.37	1.3
11	μ (10^{10} Nm^{-2})	4.8	2.82	2.28	2.08
12	v_l (m/s)	5389	4801	3856	3560
13	v_s (m/s)	3258	2925	2390	2197
14	v_m (m/s)	769.822	691.289	565.081	520.064
15	ξ	0.405	0.374	0.407	0.388
16	θ_D (K)	245.578	189.156	145.81	126.839
17	T_M (K)	1343	1024	891.821	876.956
18	f (10^5 dyne/cm)	1.998	1.382	1.188	1.138
19	v_0 (10^{12} Hz)	2.855	1.804	1.257	1.1
20	β (10^{-11} Pa^{-1})	8.231	4.883	3.985	3.577
21	C_s (10^{10}N/m^2)	4.98	3.09	2.13	2.09
22	H_v (10^9 Nm^{-2})	9.970	6.847	6.429	5.760

and covalency are effective in Sr*X*. We comment that pressure-dependent C_{ijk} behavior can have a direct means to describe the interatomic forces at high pressure. It successfully cares the short-range forces, and a balance between long-range and short-range forces.

As a next step, we intend to study the anisotropy among C_{ijk}. The equilibrium condition in the interatomic potential infers $B_1 + B_2 = -1.261\ Z_m^2$. The Cauchy discrepancy Δ_i^3 among third-order elastic constants are: (a) $\Delta_1^3 = C_{112} - C_{166} - 2P$, (b) $\Delta_2^3 = C_{123} - C_{456} - 2P$, (c) $\Delta_3^3 = -C_{144} - C_{456} - 2P$, and (d) $\Delta_4^3 = C_{123} - C_{144} - 2P$. The C_{ijk} at zero pressure, i.e., in *B*1 phase are influenced by contributions from both long-range and short-range interactions. Henceforth, Δ_i^3 is an indicator of the contribution from the non-central many-body force. Figure 6a shows the variation of Δ_i^3 as functions of pressure. The significant deviation in Δ_i^3 is a natural consequence of the non-central many-body forces as charge transfer interactions ions of Sr

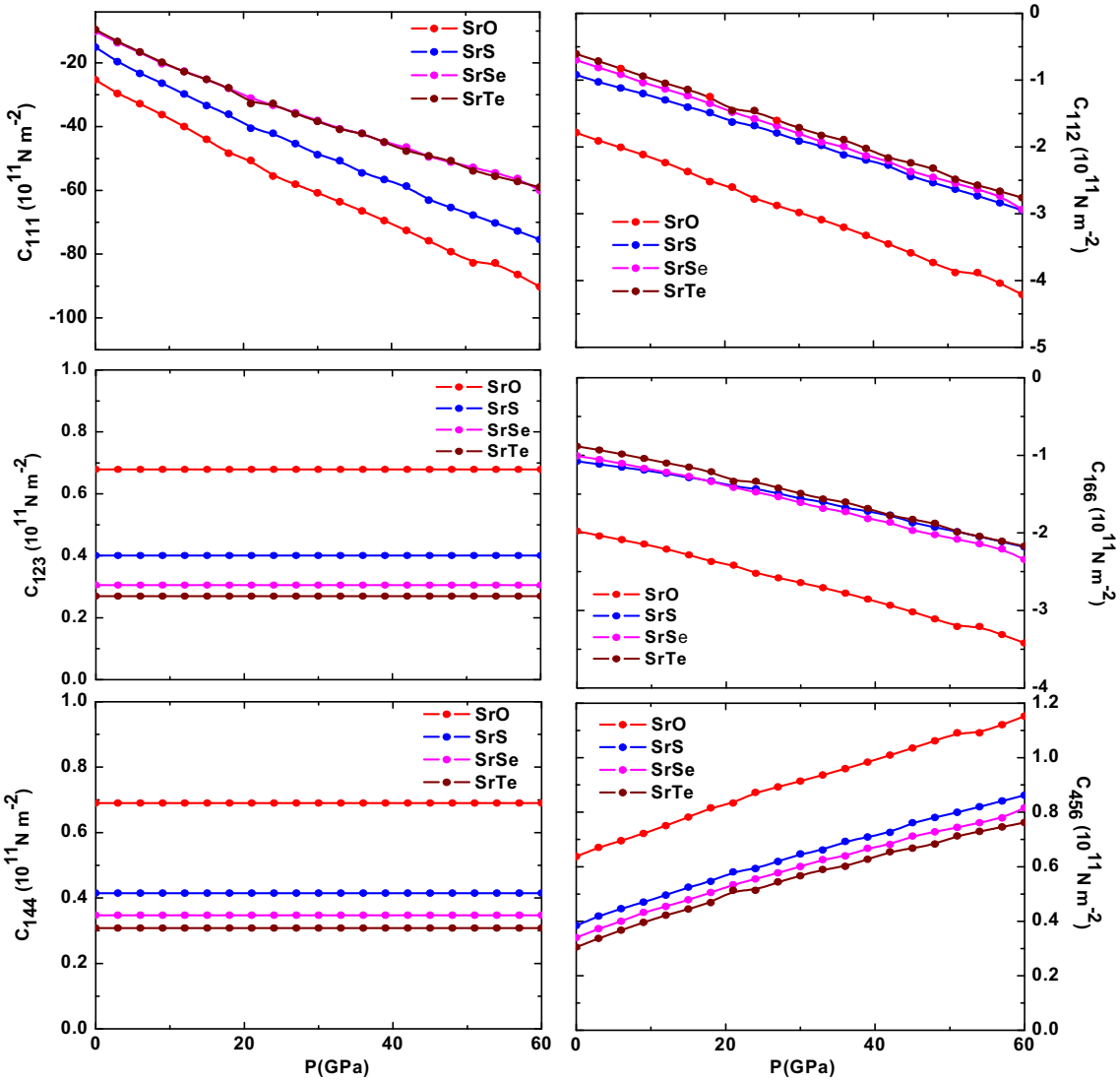

Fig. 5 Variation of aggregate third-order elastic constants (C_{ijk}) with pressure

and X atom and covalency effects caused by Sr–Sr, Sr–X, and X–X bonds apart from short-range interactions as the induced charge dipole–dipole and charge dipole–quadruple (van der Waals) interaction and the overlap repulsion. At zero pressure, Δ_2^3 and Δ_3^3 are positive, while to that Δ_1^3 and Δ_4^3 are negative in $B1$ phase. A growth in Δ_2^3 and Δ_3^3 and decay in with enhanced pressure is witnessed with enhanced pressure till phase-transition pressure. However, all Δ_i^3 is negative in $B1$ phase indicating the importance of non-central many-body forces and anharmonic effects in SrX. As far as we know, there are no experimental results available for Cauchy discrepancy Δ_i^3 in SrX.

For cubic crystal structures, the aggregate third-order elastic constants C_{ijk} discern three anisotropy coefficients and three isotropic coefficients. It is useful to express linear combinations of the anisotropy coefficients and dividing them by the isotropic coefficients. The anisotropy coefficients γ_i^3 follows:

$$\gamma_1^3 = \frac{3C_{112} - C_{111} - 12C_{144} + 12C_{166} - 16C_{456} - 2C_{123}}{2C_{123}} \tag{24}$$

$$\gamma_2^3 = \frac{C_{111} - C_{123} - 2C_{144}}{2C_{144}} \tag{25}$$

$$\gamma_3^3 = \frac{C_{166} - C_{144} - 2C_{456}}{2C_{456}} \tag{26}$$

The pressure dependence of the elastic anisotropic parameter γ_i^3 for both phases is sketched in Fig. 6b. The elastic anisotropy (γ_2^3 and γ_3^3) in $B1$ phase are less sensitive. On the other hand γ_1^3 show variation with increase in pressure in $B1$ phase. The anisotropy factor γ_1^3 is negative

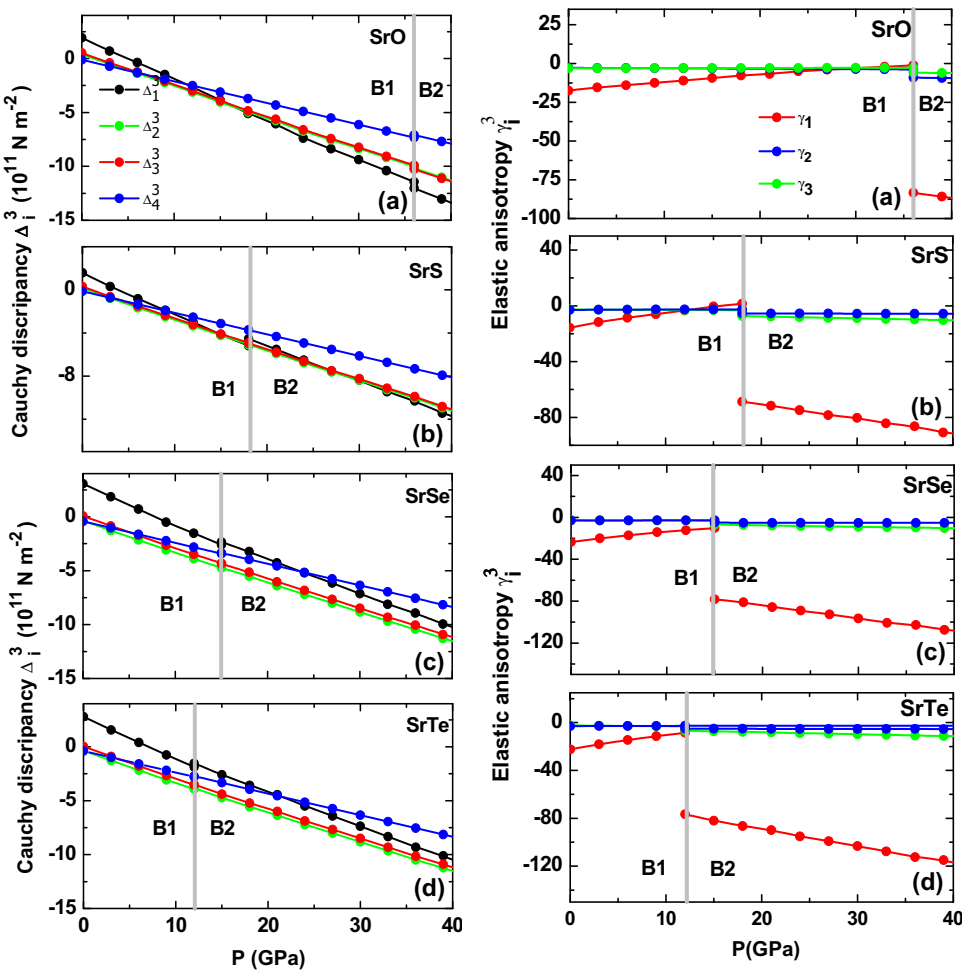

Fig. 6 Variation of Cauchy discrepancy (Δ_i^3) and elastic anisotropy (γ_i^3) in third-order elastic constant with pressure

and shows a decreasing trend with pressure in $B1$ phase at higher pressures. Value of γ_i^3 is given in Table 3 at zero temperature and pressure. As far as we know, there are no experimental and theoretical results available for comparison.

The strength and hardness are key issues for materials useful in technological applications. The mechanical strength and hardness of SrX can be known once elastic constants are known. We now determine elastic moduli at various pressures of SrX which are of substantial importance in engineering, geophysical and seismological application. The elastic properties are important in probing the bonding characteristic between adjacent atomic planes and the anisotropic character of the solid. Crystals leading to elasticity under application of pressure identify the response of a crystal under external strain. This valuable information is characterized by isotropic shear modulus (G_H), and Young's modulus (E). We note that hardness of polycrystalline materials is inhibited in elastic response as G_H and E (Fig. 7).

The resistance to volume change and resistance to reversible deformations upon applied pressures is accounted by Voigt–Reuss–Hill approximation using G_H and E following [47–49]:

$$G_H = \frac{G_V + G_R}{2} \tag{27}$$

Herein, G_V (G_R) is Voigt's (Reuss's) shear modulus corresponding to the upper (lower) bound of G_H values. The G_V (G_R) is obtained from C_{ij} assuming uniform strain throughout the sample as

$$G_V = \frac{C_{11} - C_{12} + 3C_{44}}{5} \tag{28}$$

and

$$\frac{5}{G_R} = \frac{4}{(C_{11} - C_{12})} + \frac{3}{C_{44}} \tag{29}$$

Hardness of materials is usually measured in terms of isotropic shear modulus (G_H), and Young's modulus (E) or bulk modulus (B_T). The bulk modulus infers resistance to

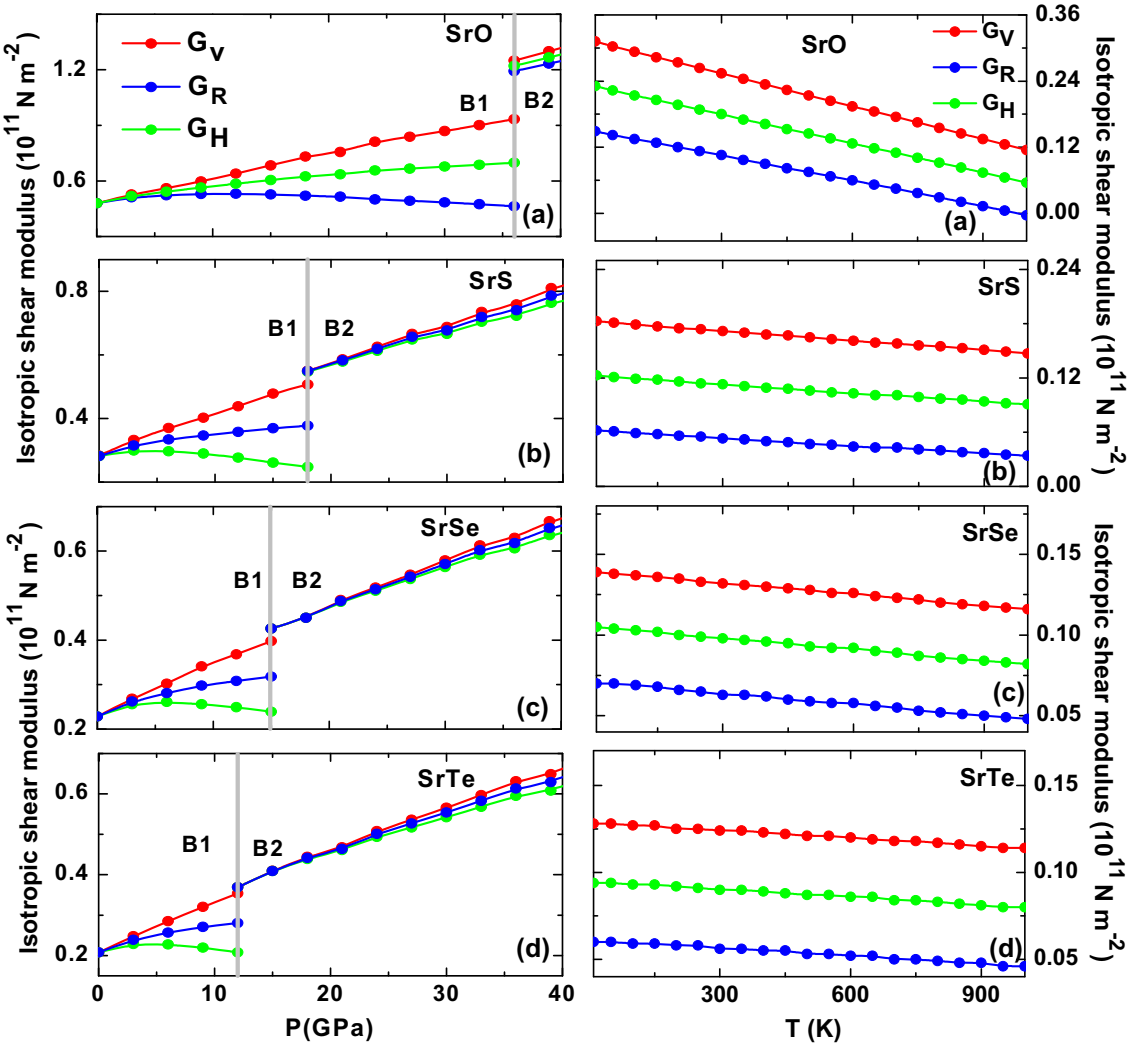

Fig. 7 Variation of isotropic shear modulus (G_H, G_V, and G_R) with pressure and temperature

volume change by applied pressure. The isotropic shear modulus (G_H) measure the resistance to reversible deformations upon shear stress. In such a situation, G_H is a better probe to measure hardness than the bulk modulus (B_T). Table 2 illustrates the calculated isotropic shear modulus (G_H), Voigt's shear modulus (G_V) and Reuss's shear modulus (G_R) for SrX at zero temperature and pressure. SrX (X = O, S Se, Te). A decreasing and then increasing nature of the isotropic shear modulus G_H, G_V and G_R is witnessed in $B1$ phase of SrX. On the other hand, a steep increase in G_H, G_V and G_R is seen with enhanced pressure in $B2$ phase at higher pressures as plotted in Fig. 7a. The explanation of the above characteristics lies in a fact that both G_V and G_R are influenced by (a) combination of C_{11}–C_{12} and (b) C_{44}. It is noticed that G_R initially decreases due to competition of these elastic constants and then start increasing above P_T in all SrX (X = O, S, Se, Te) Chalcogenides. In later phase, increasing trend in shear modulus G_H, G_V and G_R is attributed to a steep increase in $C44$ with pressure. We end up by stating that above transition pressure an increase in G_H, G_V and G_R support our earlier prediction about mechanical stiffening of lattice.

The high temperature studies of materials at ambient pressure leads to the performance of a material in terms of (a) the understanding of vibrational anharmonicity that is associated with the relative interplay of long-range and short-range potential energy function, (b) thermal response in terms of softening or hardening and (c) the elastic behavior of materials as the elasticity, extensibility, acoustic transmission velocity, Debye temperature, specific heat, and thermal conductivity.

The high temperature investigations cause laboratory difficulties as well structural changes make the phenomenon more amenable to interpretation. Figure 7b displays the G_H, G_V and G_R behavior of SrX ceramics as functions of temperature (at zero pressure). We note that

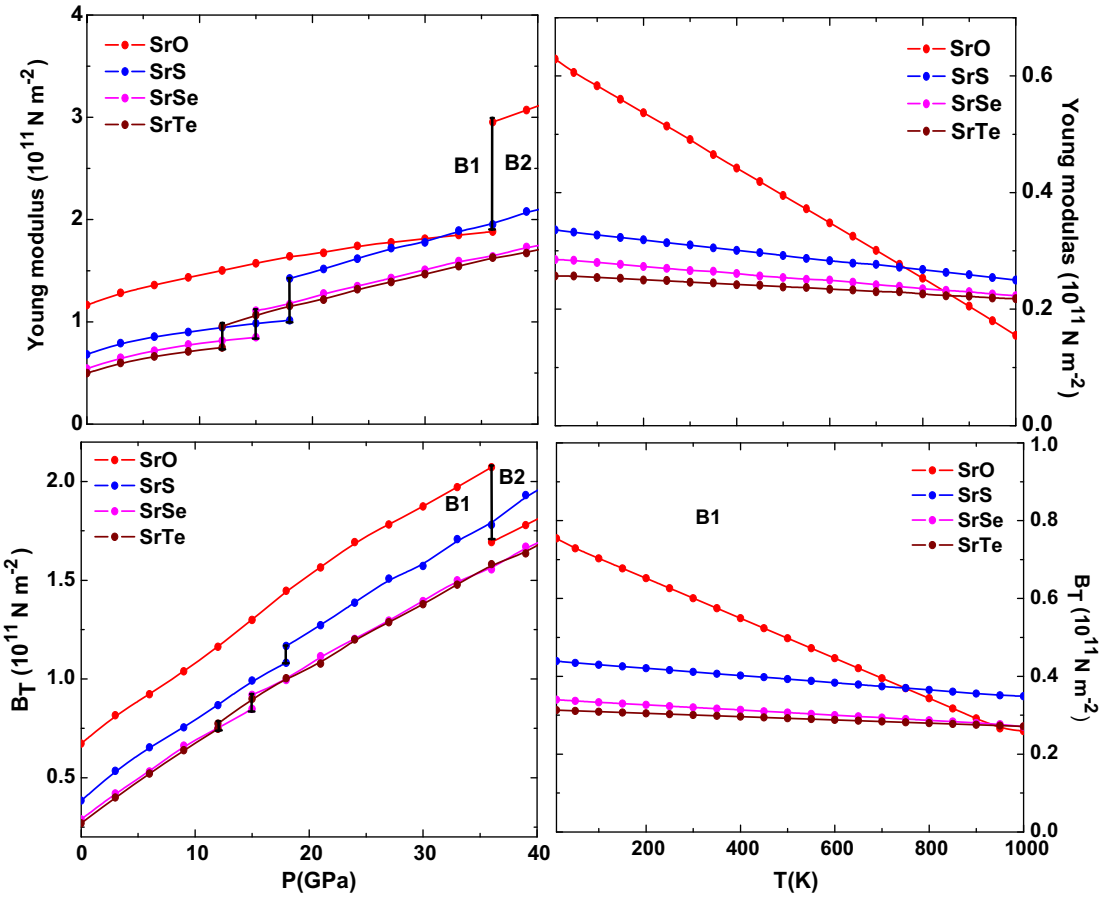

Fig. 8 Variation of Young's modulus (E) and Bulk modulus (B_T) with pressure and temperature

the isotropic shear modulus of SrX is decreasing with enhanced temperature. The steep decrease of G_H, G_V, and G_R is in accordance with aggregate second-order elastic constant C_{ij} behavior with temperature. Suppressed G_H, G_V and G_R as functions of temperature infer the weakening of the lattice as a result of thermal softening.

The tensile modulus as Young's modulus (E) further elaborates the stiffness property. E is also defined in terms of Reuss's shear modulus (G_H), and bulk modulus (B_T):

$$E = \frac{9G_H B_T}{G_H + 3B_T} \tag{30}$$

The tensile strength as Young's modulus (E), is thus computed for SrX (X = O, S, Se, Te) is illustrated in Table 2 for NaCl ($B1$) phase. It is known that the material is stiffer if its Young's modulus is high (E of steel, graphene and diamond is ~200, 1000 and 1220 GPa). Compare to these materials Sr chalcogens are less stiff. The pressure dependence of the Young's modulus (E), of SrX (X = O, S, Se, Te) is sketched in Fig. 8a. It is inferred that E enhances in $B2$ phase as compared to $B1$ phase. The calculated Young's modulus decreases as going from SrO to SrTe, and therefore, Sr chalcogenides are not stiff materials.

The temperature dependence of the tensile strength as Young's modulus (E) of SrX (X = O, S, Se, and Te) is illustrated in Fig. 8b. A decreasing trend is inferred with increase in temperature. Essentially inferring the bond expansion as well bond weakening or in other words thermal induced softening

We now make a comparison of tensile strength E (P) and E (T) of SrX (X = O, S, Se, Te). It is noted that E (P) values are smaller than E (T) for SrX at low pressures and temperatures. It implies that E (P) and E (T) are although susceptible to external variables as pressure and temperature, but it is their Sr and X (X = O, S, Se, and Te) ions in SrX (X = O, S, Se, and Te) that makes SrX (X = O, S, Se, and Te) lattice to be mechanical hard due to bond strengthening and thermal soft due to bond weakening. It is worth commenting that while tailoring the composites based on SrX, one should seek its performance in terms of tensile strength.

Another interest in SrX (X = O, S, Se, and Te).is to probe the ductile and brittle nature of Strontium and

X (X = O, S, Se, and Te) based alloys are important and predicted from the knowledge of second-order elastic constants. Ductile materials as Steel and aluminum sustains large strains before rupture, while to that brittle materials as glass and cast iron fractured at lower strains. For materials design and advances in metallurgy as well composite technology, the materials response for applied pressures and temperatures are often gauzed by stress–strain characteristics. Composites are predictive as depending on the external variable (pressure and temperature), the response of the constituent element is tailored in terms of ductile or brittle nature. Also, ductile element in composites may become brittle as the pressure or temperature is increased or decreased. Once the pressure dependence of shear modulus (G_H), and Young's modulus (E) or bulk modulus (B_T) is known, it is worth investigating ductile and brittle nature of SrX (X = O, S, Se, Te).

The shear modulus (G_H), measures the resistance to plastic deformation, while the bulk modulus (B_T) probes the resistance to fracture. An empirical relation in terms of the ratio of these moduli is known to differentiate ductile and brittle nature. In accordance, the Pugh's ratio ϕ (=B_T/G_H) >1.75, the material sustains large strains before rupture, i.e., the ductile response. On the other hand, for $\phi \leq 1.75$ the material is brittle. Empirically, 1.75 is a critical value that separates ductile and brittle response of materials [50].

From Fig. 9a, the ratio ϕ (=B_T/G_H) shows that (a) at zero pressures, semiconducting chalcogenides SrX (X = O, S, Se, Te) are ductile in NaCl phase, and (b) with increased pressure brittle nature ϕ (=B_T/G_H) >1.75 is documented but SrO shows exceptionally ductile nature in CsCl phase. Hence, semiconducting chalcogenides SrX (X = O, S, Se, Te) is ductile only at zero pressure and become brittle after structural phase transformations. To our knowledge, perovskite are ductile that is a test for its deformation before fracture. In materials performance ductility is a powerful probe for quality control. It provides a means to assess the level of impurities and proper processing of a material.

The Poisson's ratio is another measure to differentiate the ductility and brittleness of materials [51]. The critical value of Poisson's ratio (in terms of B_T and G_H) ν is 0.33 that separates ductile and brittle nature of any material. If ν >0.33, the material is ductile, and for ν <0.33, the brittle response of material is observed such as ceramics However, Poisson's ratio lies in between −1.0 and 0.5 which are the lower and upper bounds. The lower bound is a signature of the response of the materials that do not change its shape and the upper bound indicates that the volume is unchanged. The Poisson's ratio v in terms of bulk modulus B_T and the shear modulus G_H is expressed as [47–49],

$$v = \frac{1}{2}\left[3\frac{B_T}{G_H} - 2\right]\left[3\frac{B_T}{G_H} + 1\right]^{-1} \quad (31)$$

From Fig. 9a the Poisson's ratio v shows that (a) at zero pressure semiconducting SrX (X = O, S, Se, and Te) chalcogenides are brittle in nature, (b) in the NaCl phase, SrX (X = O, S Se, and Te) chalcogenides shows the brittle nature with increasing pressure, (c) at P_T, the value of v is about 0.348, 0.344, 0.333, and 0.333, for SrX (X = O, S Se, and Te) close to the brittle limit of 0.33 and (d) at high pressures, i.e., in CsCl phase again it documents the brittle nature (v <0.33). Thus, Frantsevich rule confirms the brittle nature of semiconducting SrX (X = O, S Se, Te) chalcogenides. Deduced values of v at zero pressures are about 0.212, 0.205, 0.188, and 0.192 for semiconducting SrX (X = O, S, Se, and Te) chalcogenides and As far as we know, there are no experimental and theoretical results available for comparison. It is clear that Frantsevich empirical rule classify semiconducting SrX (X = O, S, Se, and Te) chalcogenides as brittle materials. High Pugh ratio indicates the ductile nature while to that a low value infers more brittleness. There is seemingly a contradiction between Pugh's and Frantsevich empirical rules. However, these empirical rules only differ on the exact border between the bulk modulus B_T and the shear modulus G_H behavior. In view of this, semiconducting SrX (X = O, S, Se, and Te) chalcogenides can be considered a borderline case between the classes of ductile and brittle materials.

The Poisson's ratio ν and Pugh's ratio ϕ behavior as a function of temperature are sketched in Fig. 9b. The Poisson's ratio ν and Pugh's ratio ϕ is independent of temperature. Beginning from zero temperature and at high temperatures in NaCl phase, value of ν about 0.361 (SrO), 0.372 (SrS), 0.360(SrSe), 0.363 (SrTe) and the value of ϕ about 3.268 (SrO), 3.585 (SrS), 3.244 (SrSe), 3.314 (SrTe) obtained. The temperature-dependent Poisson's ratio reflects brittle nature of SrX (X = O, S Se, Te), while to that a borderline case between the classes of ductile and brittle materials is known from pressure dependence. Poisson's ratio is thus an effective indicator to control the level of impurities and processing of SrX (X = O, S, Se, and Te) ceramics. For covalent materials, v is small ($v \sim 0.1$), whereas for metallic materials v is typically 0.33. As far as we know, there are no experimental and theoretical results available for comparison.

The brittle behavior of SrX (X = O, S, Se, and Te) ceramics can also be checked by Cauchy pressures. Based on the calculated C_{12}–C_{44} for SrX (X = O, S, Se, and Te) as shown in Tables 1 and 2, it can be seen that the Cauchy pressures are negative. These results again indicate that SiC is brittle in nature. Furthermore, the Poisson's ratio ν is used as a probe to identify the bonding characteristic of the forces than any of the other elastic constants. Estimated

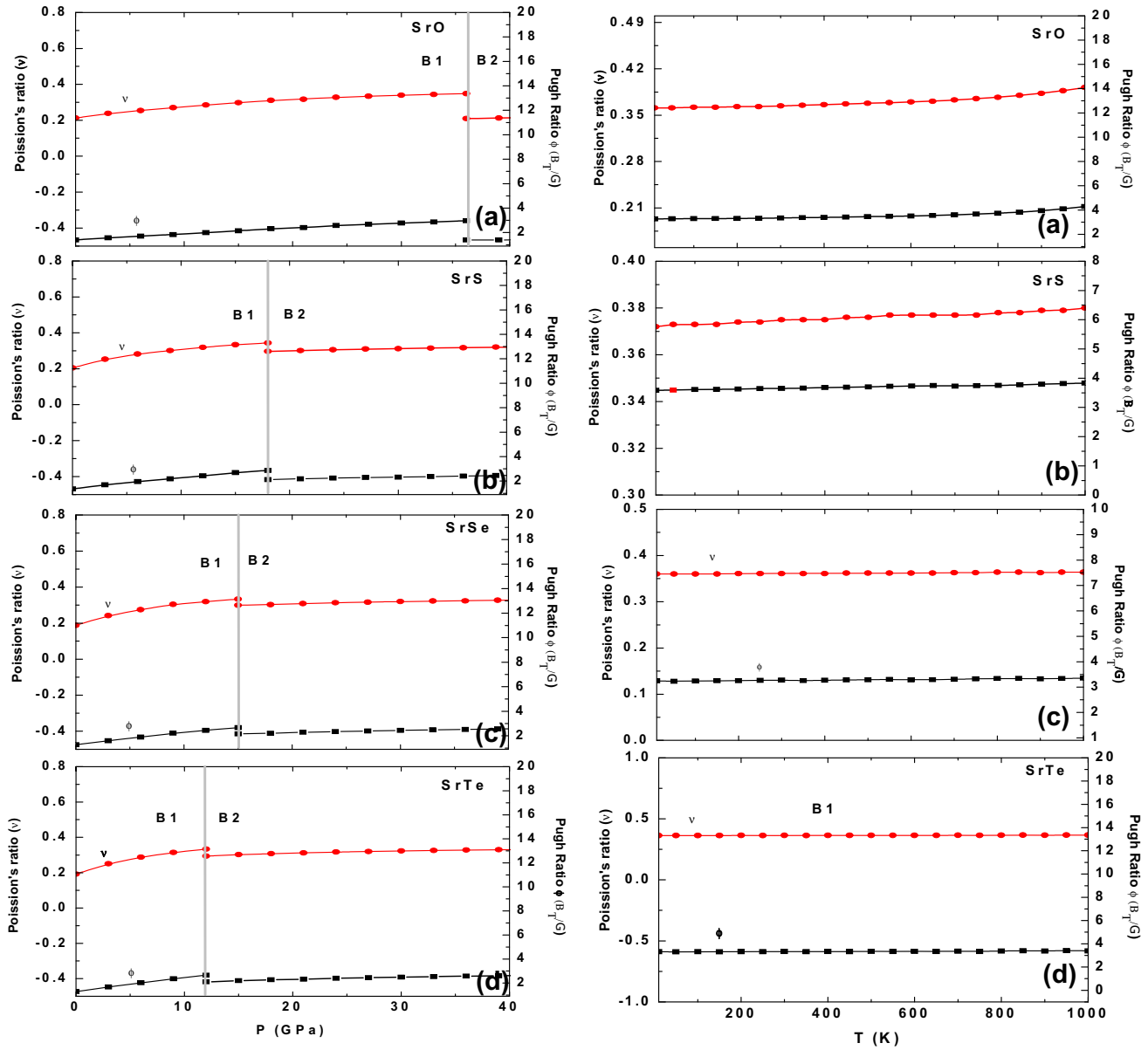

Fig. 9 Variation of Poisson's ratio (ν) and Pugh's modulus ratio (Φ) with pressure and temperature

Poisson's ratio is close to 0.25, which means that SrX (X = O, S, Se, and Te) are with predominantly central inter-atomic forces. The larger the Poisson's ratio is, the better the plasticity is henceforth, SrX (X = O, S, Se, and Te) is the one which shows a better plasticity.

Usually, the elastic moduli describe only reversible response of a material to small strain near equilibrium. The intrinsic strength of a material reflects permanent plastic deformation at large shear strain. Consequently, to further understand the behavior of SrX (X = O, S, Se, and Te) in terms of Vickers hardness: $H_V = 2\ (\phi^2 G_H)^{0.585} - 3$. Here, $\phi = B_T/G_H$. Figure 10a illustrates the theoretical Vickers hardness as a function of pressure. It is clear from the plot that the Vickers hardness H_V decreases in $B1$ phase and then increases in $B2$ phase with increase in pressure, which indicates that SrX (X = O, S Se, and Te) becomes hard under pressure implying its good mechanical properties. Figure 10b showed Vickers hardness as a function of temperature for SrX (X = O, S, Se, and Te). It is clear from the plot that the Vickers hardness H_V decreases in $B1$ phase, which indicates that SrX (X = O, S, Se, and Te) gets softened with enhanced temperature. Apart from the elastic anisotropy of crystals, the hardness is important to discuss their properties because it is highly correlated with the possibility of inducing micro cracks in materials.

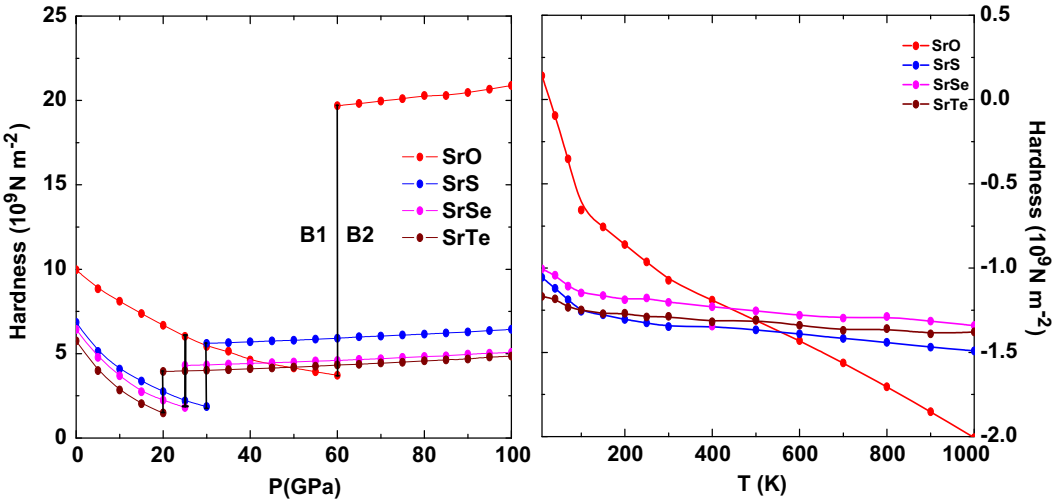

Fig. 10 Variation of hardness (H_V) as a function of pressure and temperature

SrX (X = O, S, Se, and Te) are promising materials with wide range of applicability's with effective mechanical properties. Usually, materials elastic properties are a source of valuable information where materials mechanics is significant as the knowledge of deformational characteristics of materials is essential in engineering design and construction of effective structures. Having, understood the materials elastic behavior using Bulk modulus (B_T), shear modulus (G_H, G_V and G_R), and Young modulus (E), in the following, we will use our calculated elastic constants to discuss the compressional and shear wave velocity in semiconducting SrX (X = O, S, Se, and Te). The velocities of the longitudinal v_l and shear waves v_s are known from the Lamé's constants, λ and μ. The compressional wave with velocity v_l propagates back and forth in a crystal. The shear wave with velocity v_s goes up and down.

The Lamé's constants are related to Young's modulus (E) and Poisson's ratio (ν) (correlating the bulk modulus B_T and the shear modulus G_H). The first Lamé's constant (λ) measures the compressibility of the material. The second Lamé's constant (μ) infers its shear stiffness [47–49]. The Lamé's constants (λ and μ) are expressed as:

$$\lambda = \frac{vE}{(1+v)(1-2v)} \tag{32}$$

$$\mu = \frac{E}{2(1+v)} \tag{33}$$

Figure 11a displays the pressure dependence of the first and second Lamé's constants (λ, μ). Starting from zero pressure and at high pressures, both Lamé's constants (λ, μ) are positive. Note that the Lamé's constant (λ) can be negative, however, for most materials it is also positive. The second Lamé's constant (μ) is positive. An increasing trend of compressibility (λ) of SrX (X = O, S, Se, Te) is witnessed in terms of λ as seen in both rock salt and CsCl structures and is attributed to mechanical hardening of lattice. The decreasing trend in $B1$ phase and increasing trend in $B2$ phase of shear modulus (G_H, G_V and G_R) results in a decreasing behavior of shear stiffness (μ) in $B1$ phase and then enhanced shear stiffness in $B2$ phase. Note that λ and μ together constitute a parameterization of the elastic moduli for homogeneous isotropic media.

The value of pressure-dependent Lamé's constants (λ, μ) is documented in Table 3. Deduced values of Lamé's constants (λ, μ) could not be compared due to lack of data on SrX (X = O, S, Se, and Te). Figure 11b summarizes the temperature-dependent behavior of Lamé's constants (λ, μ), for SrX (X = O, S, Se, and Te). It is noticed that both Lamé's constants (λ, μ) are decreasing with increasing temperature. Thus, both compressibility and shear stiffness showed decreasing trend with temperature variations and identifies once again the thermal softening of SrX (X = O, S, Se, and Te).

The Lamé's constants (λ, μ) determines the longitudinal (shear) wave velocity as

$$v_l = \left[\frac{\lambda + 2\mu}{\rho}\right]^{\frac{1}{2}} \tag{34}$$

$$v_s = \left[\frac{\mu}{\rho}\right]^{\frac{1}{2}} \tag{35}$$

Here, ρ is the density. The average wave velocity v_m has been approximately given by

$$v_m = \left[\frac{1}{3}\left(\frac{2}{v_t^3} + \frac{1}{v_s^3}\right)\right]^{-\frac{1}{3}} \tag{36}$$

The compressional longitudinal (shear) wave velocity thus depends on density of the material as well on Bulk

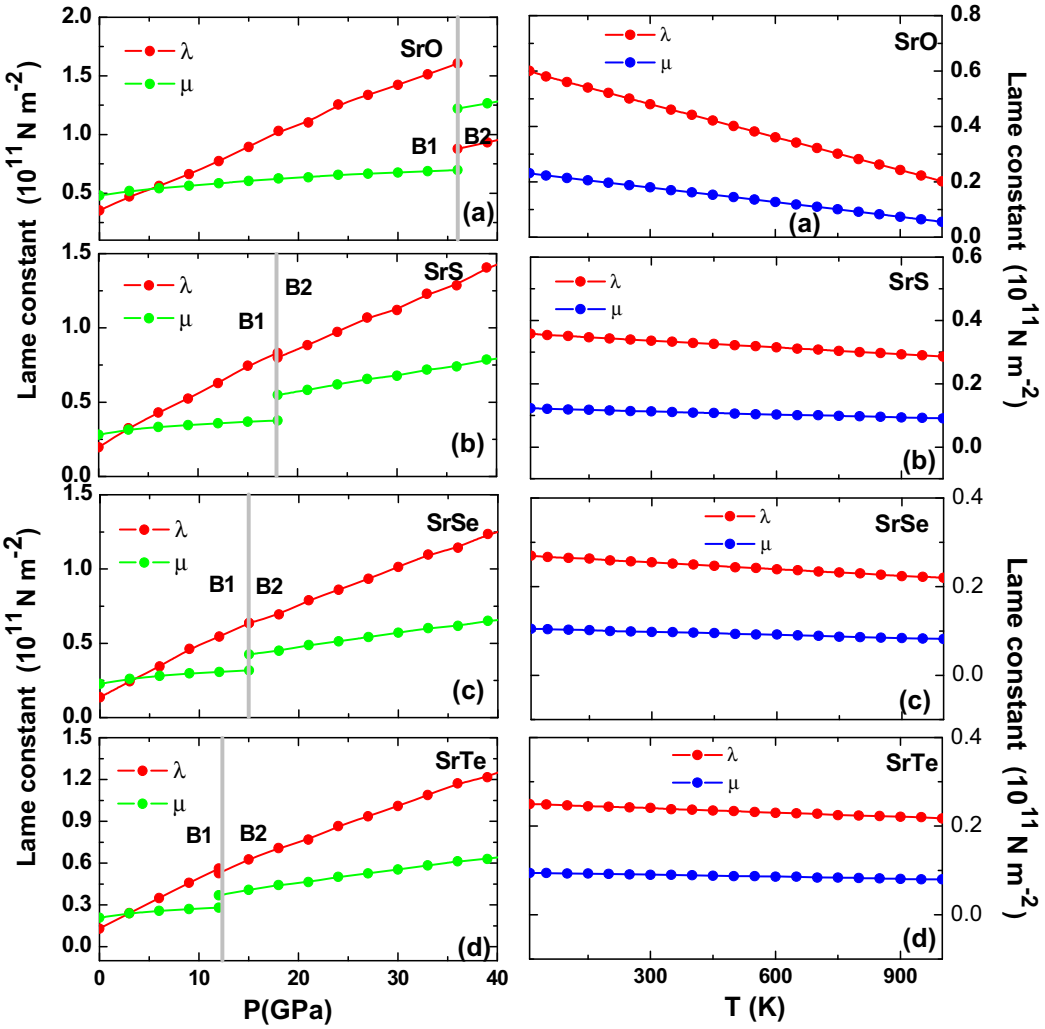

Fig. 11 Variation of Lamé's constant (λ, μ) with pressure and temperature

modulus (B_T), shear modulus (G_H, G_V and G_R), and Young modulus (E). We note that Bulk modulus (B_T) has a strong dependence on the density of the material; Young modulus (E) displays a weak dependence, while the shear modulus (G_H) is independent of density.

Figure 12a displays the pressure dependence of the longitudinal (shear) wave velocity in SrX (X = O, S, Se, Te). In rock salt phase, beginning from zero pressures and at high pressures, compressional wave velocity v_l increases while to that shear wave velocity v_s decreases. Both compression and shear waves increases with enhanced pressure in $B2$ structure. Deduced values of longitudinal, shear and average elastic wave velocities propagating in SrX (X = O, S, Se, and Te) are illustrated in Table 3 at zero temperature and pressure. Figure 12b represents the temperature dependence of the longitudinal (shear) velocity, respectively. It is noticed that both longitudinal (shear) wave velocity decreases in $B1$ phase with enhanced temperature. The values of the longitudinal, shear and average elastic wave velocities propagating in SrX (X = O, S, Se, Te) are documented in Table 4 at room temperature. The high temperature behavior of longitudinal (shear) wave velocity for SrX (X = O, S, Se, and Te) can be considered as predictive studies as they cannot be compared due to unavailability of high temperature data.

The Navier's equation is also used to determine the longitudinal and the shear wave velocity [52, 53]. These are written in terms of Reuss's shear modulus (G_H), and bulk modulus (B_T) as

$$v_l = \left[\frac{3B_T + 4G_H}{3\rho}\right]^{\frac{1}{2}} \tag{37}$$

$$v_s = \left[\frac{G_H}{\rho}\right]^{\frac{1}{2}} \tag{38}$$

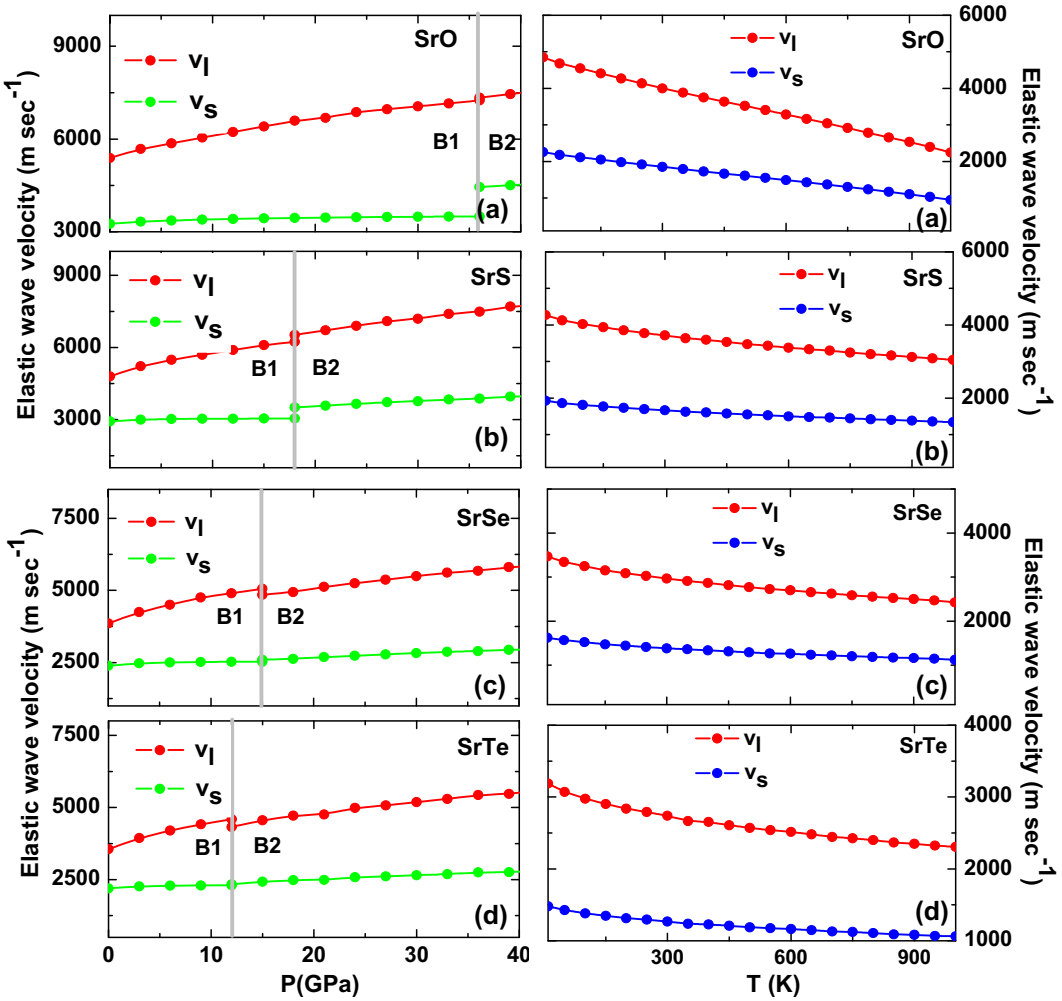

Fig. 12 Variation of elastic wave velocity v_l and v_s with pressure and temperature

Elastic, plastic and molten state properties with pressure as controlling variable are useful for tailoring composites. The Lamé's constants (λ, μ) are of substantial interest for plastic materials. Referring to Eqs. 32 and 33, we note that as the Poisson's ratio (ν) increases, the Lamé's constant (λ, μ) numerically approach the bulk modulus (E). For fluids, the Reuss's shear modulus (G_H) vanishes as the viscosity of the fluid approaches zero. The above is important in context of the present computation and can also be cross-checked from the relation between bulk modulus and Reuss's shear modulus: $B_T = \lambda + 2\ G_H/3$. Furthermore, G_H approaches zero for fluids and hence the Poisson's ratio is ~ 0.5.

The response to deformations against bond bending or bond-angle distortion is relevant for materials with promising technological applications and also a test to validate the many-body non-central potential that we dealt with. The aggregate elastic constants infers the elastic properties of material that undergo stress, deform and then recover after returns to its original shape after stress ceases. The nature of elastic constants in solids holds a great importance to elucidate the microscopic nature interatomic bonding, equations of state, and vibrational density of states. The above can be understood in terms of Kleinman parameter ξ which describes the relative positions of the cation and anion sub lattices under volume-conserving strain distortions for which positions are not fixed by symmetry [54, 55]. We have explored its applicability to ceramics SiC by using [56]

$$\xi = \frac{C_{11} + 8C_{12}}{7C_{11} + 2C_{12}} \tag{39}$$

The pressure dependence of Kleinman parameter ξ is sketched in Fig. 13c for SrX (X = O, S, Se, and Te) in rock salt ($B1$) and CsCl ($B2$) phases Deduced value of ξ about 0.405 (SrO), 0.374 (SrS), 0.407 (SrSe), 0.388 (SrTe) is documented in Table 3 for SrX (X = O, S, Se, and Te) at zero temperature and pressure. The value of ξ about 0.339

Table 4 Calculated aggregate second-order elastic constants (C_{11}, C_{12} and C_{44}) and aggregate bulk modulus (B_T), average elastic constant (Cs) second-order elastic constant anisotropy parameter (γ_i^2), isotropic shear modulus (G_H), Voigt's shear modulus (G_V), Reuss's shear modulus (G_R), Young's modulus (E), Poisson ratio (ν), first and second-order Lame's constant (λ, μ), longitudinal (v_l), shear (v_s) and average elastic wave velocity (v_m), Kleinman parameter (ξ), Grüneisen parameter (γ_G), and hardness (H_v), thermo dynamical properties: Debye temperature (θ_D), melting temperature of SrX (X = O, S, Se, and Te) in *B1* phase. at temperature of about 300 K

S. no.	Elastic properties	SrO	SrS	SrSe	SrTe
1	C_{11} (10^{10} Nm^{-2})	13.09	9.16	6.76	6.40
2	C_{12} (10^{10} Nm^{-2})	2.46	1.59	1.42	1.31
3	C_{44} (10^{10} Nm^{-2})	0.69	0.34	0.42	0.37
4	B_T (10^{10} Nm^{-2})	6.01	4.11	3.20	3.00
5	C_S (10^{10} Nm^{-2})	5.32	3.79	2.67	2.55
6	γ_1^2	6.703	10.132	5.357	5.878
7	G_H (10^{10} Nm^{-2})	1.8	1.13	0.98	0.9
8	G_V (10^{10} Nm^{-2})	2.54	0.53	1.32	1.24
9	G_R (10^{10} Nm^{-2})	1.06	1.72	0.63	0.56
10	E (10^{10} Nm^{-2})	4.91	3.1	2.66	2.46
11	v	3.64	0.375	0.361	3.64
12	λ (10^{10} Nm^{-2})	4.8	3.36	2.55	2.41
13	μ (10^{10} Nm^{-2})	2.31	1.13	0.98	0.9
14	v_l (m/s)	4001	3714	2965	2739
15	v_s (m/s)	1852	1663	1381	1268
16	v_m (m/s)	448.2	403.7	335.2	308.0
17	ξ	0.339	0.325	0.361	0.356
18	θ_D (K)	163.514	128.1, 353.6 [10]	103.9	90.209
19	T_M (K)	1327	1094	952.603	931.202
20	H_v (10^9 Nm^{-2})	0.140	−1.188	−1.107	−1.233
21	γ_G	1.54	1.51, 1.64 [10]	1.41	1.43

(SrO), 0.325 (SrS), 0.361 (SrSe), 0.356 (SrTe) is obtained at room temperature and is reported in Table 4 for SrX (X = O, S, Se, and Te). As far as we know, there is no experimental result available for Kleinman parameter and is considered as a prediction study. For both rock salt and CsCl structures, the knowledge of elastic constants at variable pressure is worth investigating aimed for practical applications related to the mechanical properties of a solid: load deflection, thermo elastic stress, internal strain, elastic wave velocities, and fracture toughness.

Physical properties as thermal expansion, heat capacity and Grüneisen parameter can be explained with higher order terms of the interaction potential. The thermal process in terms of heat conduction is hindered if one considers a solid to be perfect harmonic and thermal conductivity will be infinitely large. Thus, the role of anharmonic effects or phonon decay is important as enhanced pressures as well temperatures allows a change in volume or dimensions. The pressure-dependent calculations of elastic constants will provide measures of the accuracy of the calculation of forces in SiC as well the mechanical stiffening or hardening attributed to Sr–Sr, X–X, and Sr–X bond compression and bond strengthening due to lattice vibration.

We express the molecular force in the absence of the Lorentz effective field [23–37]

$$f = \frac{1}{3}\left[\frac{\mathrm{d}^2}{\mathrm{d}r^2}U_{\mathrm{SR}}(r) - \frac{2}{r_0}\frac{\mathrm{d}}{\mathrm{d}r}U_{\mathrm{SR}}(r)\right]_{r=r_0}, \tag{40}$$

The force constant is a function of the second-order derivatives of the short-range (SR) overlap repulsive potential and as well the charge dipole–dipole and charge dipole–quadruple van der Waals potential. The Reststrahlen frequency is obtained from the force constant using

$$\upsilon_0 = \frac{1}{2\pi}\left[\frac{f}{\mu}\right]^{1/2}, \tag{41}$$

Here, μ is the reduced mass of SrX (X = O, S, Se, Te).

The Grüneisen parameter γ_G is a ratio of second and first-order derivatives of the potentials enable us to discuss the anharmonic effects in a crystal. We express γ_G as

$$\gamma_G = -\frac{r_0}{6}\left[\frac{U'''(r_0)}{U''(r_0)}\right] \tag{42}$$

The pressure dependence of Grüneisen parameter is sketched in Fig. 13a for SrX (X = O, S, Se, Te) in rock salt ($B1$) and CsCl ($B2$) phases. A linear decrease of γ_G with pressure in both phases is observed. Deduced γ_G value of about 1.523(SrO), 1.508(SrS), 1.403(SrSe), 1.425(SrTe) in NaCl ($B1$) phase. On the other hand, Fig. 13b discerns temperature dependence of Grüneisen parameter with a

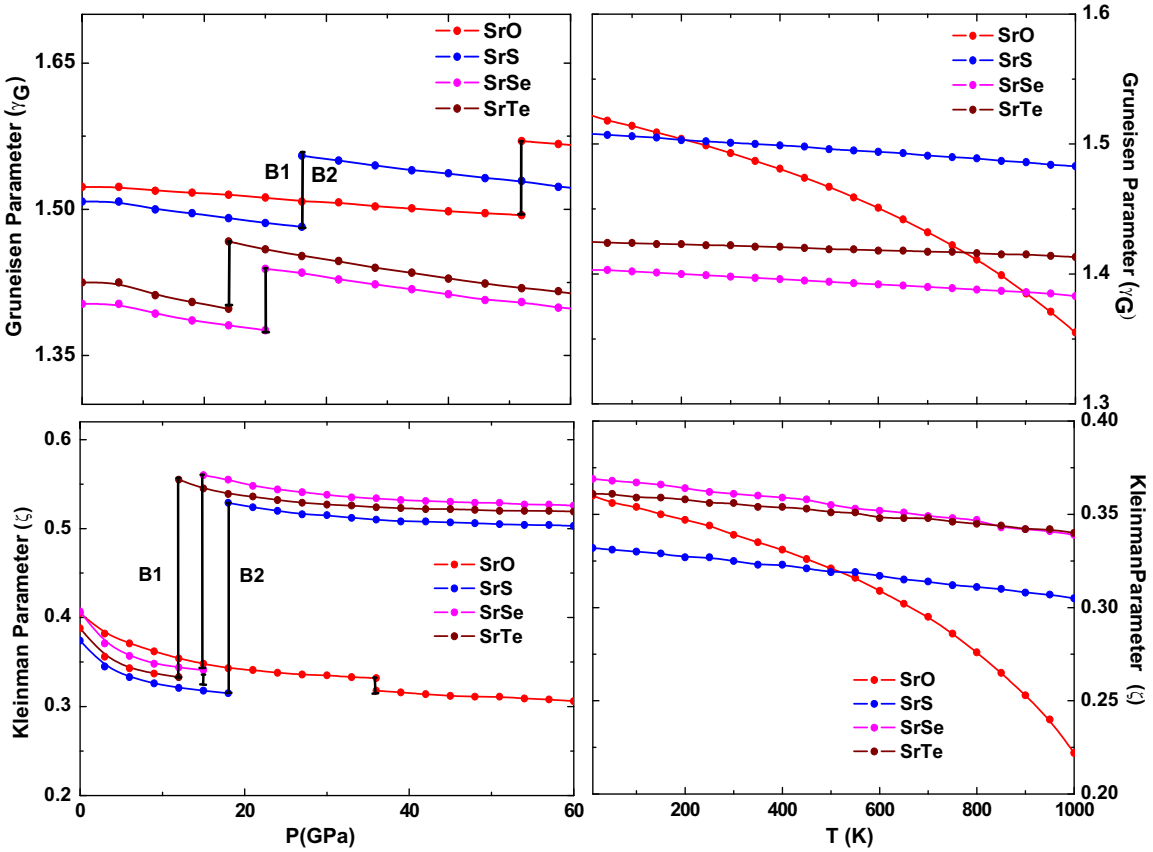

Fig. 13 Variation of Grüneisen parameter (γ_G) and Kleinman parameter (ξ) with pressure and temperature

value of about 1.54 (SrO), 1.51 (SrS), 1.41 (SrSe), 1.43 (SrTe) at 300 K which is comparable with available theoretical result of 1.64 (SrS) [10] As far as we know, there is no experimental result available for Grüneisen parameter and is considered as a prediction study. For most of the solids, Grüneisen parameter ranges from 1.5 to 2.5. As Grüneisen constant γ_G behavior is influenced by ratio of second and first-order derivatives of the potentials, we may thus comment that anharmonicity is significant in SrX (X = O, S, Se, Te). Note that these results are further validated by inelastic neutron scattering measurements to probe phonon frequencies as a function of the crystal volume.

We further compute Debye temperature (θ_D) to shed further light on mechanical stiffened and thermal softened characteristics of SrX following [57–61]:

$$\theta_D^3 = \frac{3.15}{8\pi}\left(\frac{h}{k_B}\right)^3\left(\frac{r}{M}\right)^{\frac{3}{2}}\left(\frac{C_{11}-C_{12}}{2}\right)^{\frac{1}{2}}\left(\frac{C_{11}+C_{12}+2C_{44}}{2}\right)^{\frac{1}{2}}C_{44}^{\frac{1}{2}}, \tag{43}$$

where M is the acoustic mass of SrX. The notations h and k_B are the Planck and Boltzmann constants.

The Debye temperature as functions of pressure is plotted in Fig. 14a for SrO, SrS, SrSe, and SrTe. At zero pressure, θ_D is about 246 (SrO), 189 (SrS), 146 (SrSe), 127 (SrTe) K. It is noticed that with enhanced pressure, θ_D increases in $B1$ phase for SrX (X = O, S, Se, Te). The Debye temperature from $B1$ to $B2$ phase is jumped by 45 (SrO), 40 (SrS), 23 (SrSe), 20 (SrTe) K at P_T. On the other hand, θ_D also showed an increase in $B2$ phase. Deduced value of θ_D at zero pressure is listed in Table 3. Enhanced θ_D in $B1$ phase at higher pressure indicates the mechanical stiffening of lattice.

Deduced value of θ_D at 300 K is listed in Table 4. Debye temperature is a function of temperature and its value varies from technique to technique as well depends on the sample quality. Usually, a standard deviation in θ_D of about 25 K is agreeable. The change in the force constants induced by pressure increases θ_D in $B1$ phase and after transition pressure it continue to increasing which drives the system effectively towards the stiffening of lattice with increasing pressure.

Figure 14b displays the variation of the Debye temperature as functions of temperature at zero pressure. Starting from zero temperature, θ_D decreases rapidly. On the other hand, θ_D enhances with applied pressures at zero temperature. It is worth commenting from high-pressure and high-temperature Debye temperature behavior that (a) the

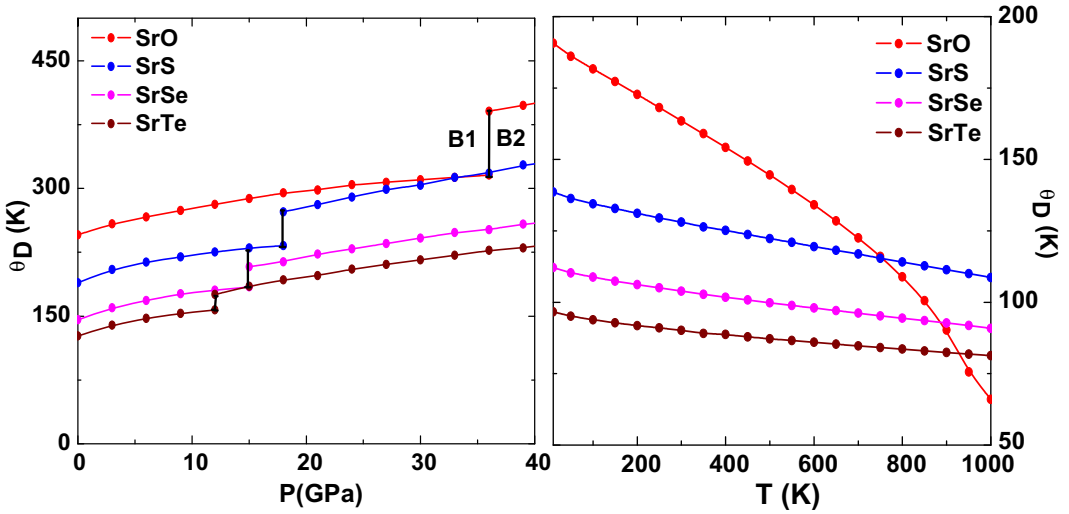

Fig. 14 Variation of Debye temperature (θ_D) as a function of pressure and temperature

pressure-dependent Debye temperature infers the mechanical stiffened bulk modulus due to Sr–Sr, *X*–*X*, and Sr–*X* bond compression and bond strengthening due to lattice vibration and (b) the thermal softening of bulk modulus results from bond expansion and bond weakening due to thermal stress in Sr*X* (*X* = O, S, Se, Te) in rock salt structure.

A comparison of values of $\theta_D(P)$ and $\theta_D(T)$ at zero pressure and zero temperature results: $\theta_D(P) > \theta_D(T)$ implying the susceptibility of θ_D with pressure. It is worth to comment that $\theta_D(P)$ and $\theta_D(T)$ behave differently with applied pressure and temperatures in Sr*X* (*X* = O, S, Se, and Te). This is attributed to the fact vibrational spectrum of Sr*X* (*X* = O, S, Se, and Te) lattice is controlled by aggregate elastic constants C_{ij} behavior. Thus, the understanding of Debye temperature behavior of a material not only provides essential features of the vibrational spectrum but is also mandatory for technological and engineering applications. This quantity is useful as a reference for future experimental studies.

The cumulative effect of both pressure and temperature led us to define aggregate elastic constants C_{av} as

$$C_{av} = \left(\frac{8\pi}{3.15}\right)^{\frac{2}{3}} \left(\frac{k_B}{h}\right)^2 \left(\frac{M}{r}\right) \theta_D^2, \tag{44}$$

This is useful once Debye temperature at zero pressure is known from experiments. Despite various investigations on mechanical and thermodynamical properties, basic properties controlled by elastic constants related with high temperature behaviors are lacking.

To further explore the role of anharmonic effects in terms of heat capacity at constant volume C_v and thermal expansion coefficient α, we express the vibration term A_{vib} [62, 63]:

$$A_{vib}(\theta_D, T) = nk_BT\left[\frac{9\theta_D}{8T} + 3\ln\left\{1 - \exp\left(-\frac{\theta_D}{T}\right)\right\} - D(\theta_D/T)\right] \tag{45}$$

The non equilibrium Gibbs function, $G^*(V; P, T)$, is minimized with respect to volume *V* as

$$\left[\frac{\partial G^*(V;P,T)}{\partial V}\right]_{P,T} = 0 \tag{46}$$

From Eq. (47), we determine heat capacity at constant volume C_v as

$$C_v = 3nk_B\left[4D\left(\frac{\theta_D}{T}\right) - \frac{3\theta_D/T}{e^{\theta_D/T} - 1}\right] \tag{47}$$

Figure 15a documents the variations of heat capacity at constant volume, C_v, with pressure *P* for both *B*1 and *B*2 phase of Sr*X* (*X* = O, S, Se, and Te) at *T* = 50, 100, 300 and 500 K. The normalized heat capacity is $[C_v(P) - C_v(0)]/C_v(0)$, where $C_v(P)$ and $C_v(0)$ are heat capacity at any pressure *P* and at zero pressure. Starting from zero pressure, normalized heat capacity decreases gradually with enhanced pressure in *B*1 phase. This behavior essentially point to the fact that the Sr*X* (*X* = O, S Se, and Te) lattice vibrations energy are controlled by both pressure as well temperature. Note that for higher temperatures $T \rightarrow \theta_D$, the variation in heat capacity with pressure is weak in *B*1 phase. Also, at P_T, reduced jump in between rock salt and CsCl structures can be seen as compared to low temperatures. Similar observations are previously reported on SrO following quasi-harmonic approximation in explaining the thermal expansion coefficient, specific heat, entropy, bulk modulus and the thermal Grüneisen parameter with temperature and pressure in both phases [64].

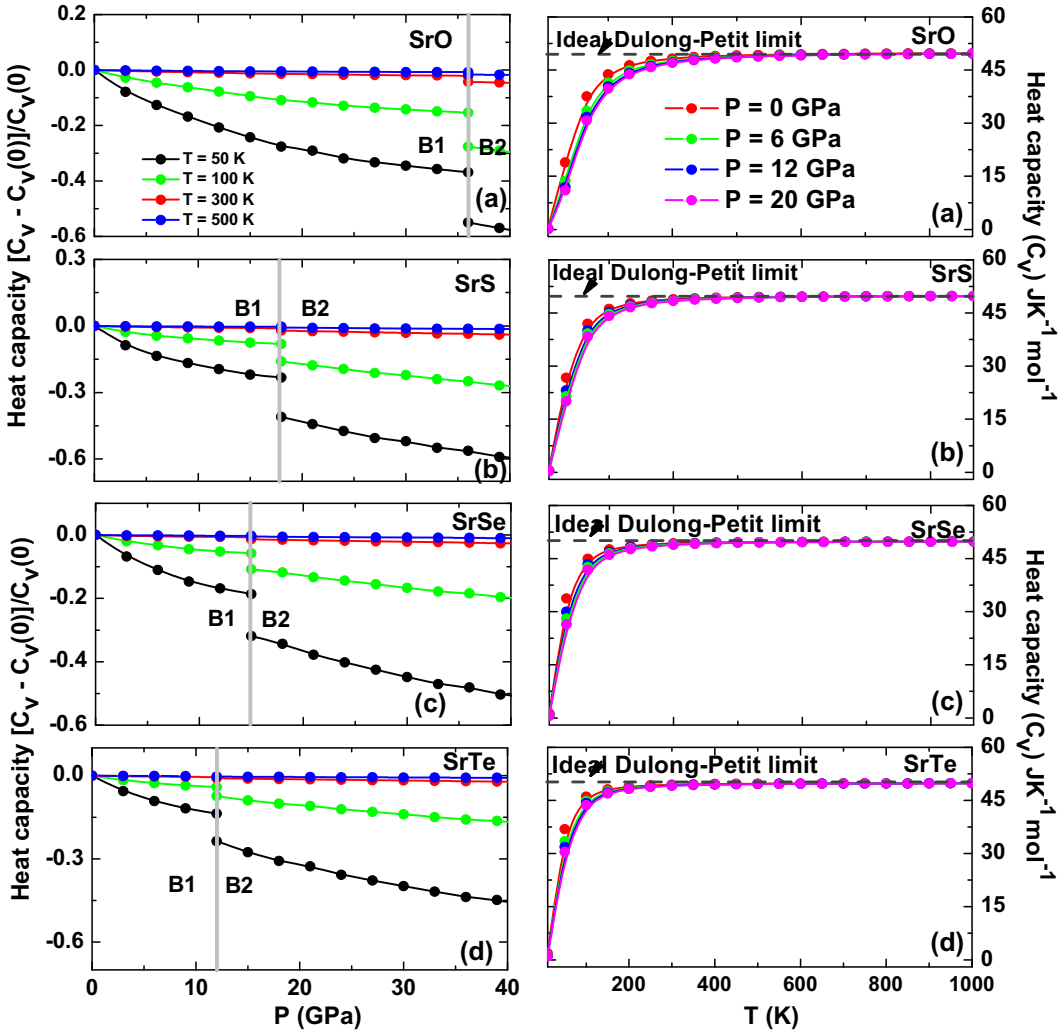

Fig. 15 Variation of heat capacity (C_v) with pressure at different temperatures and with temperature at different pressures

The Debye temperature calculated from elastic constants must have a close resemblance as to measure from specific heat measurements only at low temperatures. It is instructive to study the temperature-dependent behavior of heat capacity. Figure 15b illustrates the heat capacity at constant volume, C_v, behavior as functions of temperature for various pressures (0, 6, 12, 20 GPa) within the framework of quasi-harmonic model for SrX (X = O, S, Se, Te). It can be seen that below room temperature (300 K), C_v increases very rapidly with the temperature at all pressures. Above room temperature, C_v increases slowly with the temperature. It almost approaches a constant ideal gas limit—the Dulong–Petit limit, $C_v(T) = 3\ R$, at higher temperatures as well at all pressures for SrX (X = O, S, Se, and Te).

We further determine thermal expansion coefficient $\alpha_{th.exp}$ using Eq. (47) as

$$\alpha_{th.exp} = \frac{\gamma C_v}{B_T V} \tag{48}$$

Apart from the pressure dependence of heat capacity at constant volume C_v, the Grüneisen parameter and Bulk modulus is also needed to elucidate the thermal expansion coefficient ($\alpha_{th.exp}$). It is a measure of any alteration in phonon frequency depending on the lattice's expansion or contraction in volume as a result of temperature variation. Figure 16a illustrates the pressure dependence of $\alpha_{th.exp}$. For SrX (X = O, S, Se, and Te) in both rock salt and CsCl, i.e., $B1$ and $B2$ phase. A nonlinear decrease in $\alpha_{th.exp}$ is thus witnessed with pressure in both NaCl and CsCl phase. The decrease is more rapid in rock salt structure while a slow decrease is documented in CsCl structure. We note that at P_T, the thermal expansion coefficient $\alpha_{th.exp}$ is suppressed by 10–20 % in SrX (X = O, S, Se, Te) at temperatures 50, 100, 300, and 500 K, respectively.

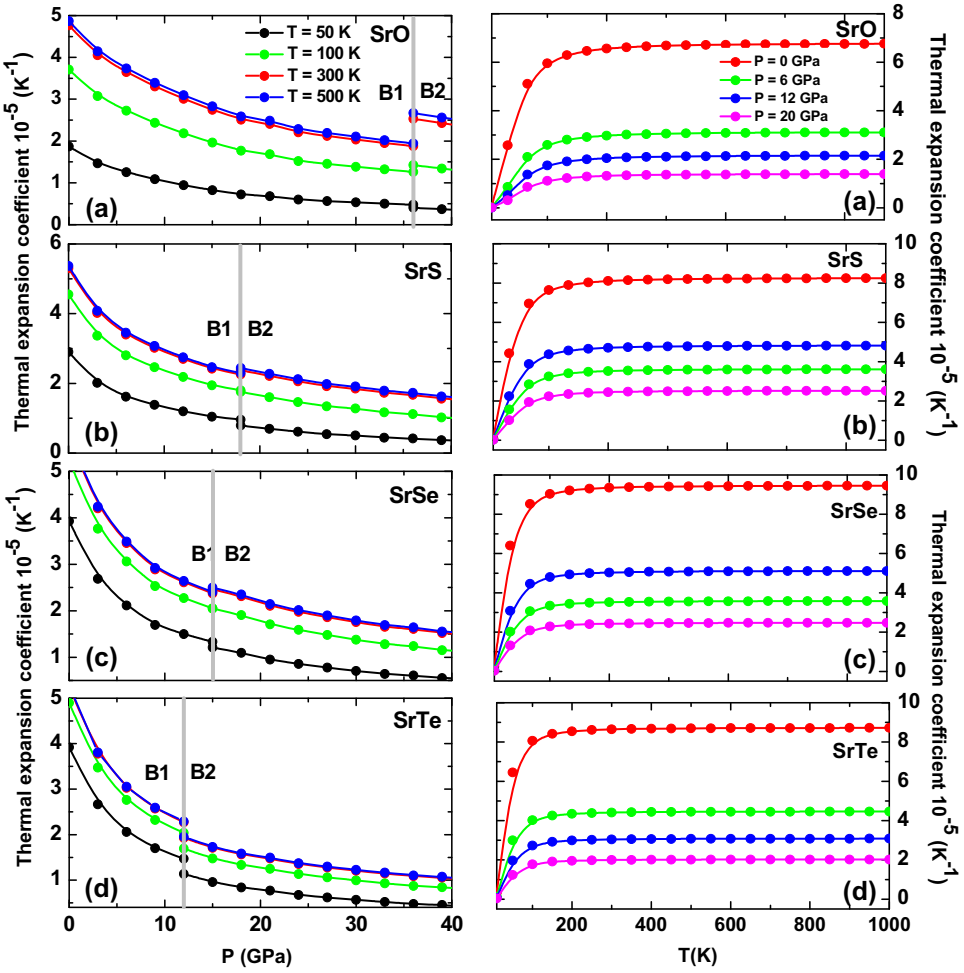

Fig. 16 Variation of the thermal expansion coefficient ($\alpha_{th.exp}$) with pressure at different temperatures and with temperature at different pressures

The variations of $\alpha_{th.exp}$ as functions of temperature at various pressures have been plotted in Fig. 16b for SrX (X = O, S, Se, and Te). This figure shows that at low temperatures ($T < 200$ K), $\alpha_{th.exp}$ enhances rapidly with temperature at $P = 0$ and 20 GPa. At high temperatures (T > 200 K), a sharp increase of $\alpha_{th.exp}$ is witnessed at all pressures. This figure also suggests that with enhanced pressure, the increase of $\alpha_{th.exp}$ with temperature becomes smaller. In other words, the slope of $\alpha_{th.exp}$ gradually decreases at higher temperatures at all pressures except at $P = 0$ GPa. Returning back to pressure dependence of thermal expansion coefficient ($\alpha_{th.exp}$), we note a rapid decrease in rock salt structure with the increase of pressure. A comparison of $\alpha_{th.exp}$ (P) and $\alpha_{th.exp}$ (T) reveals that $\alpha_{th.exp}$ (P) values are smaller than that $\alpha_{th.exp}$ (T) for SrX (X = O, S, Se, and Te) under same pressure and temperature. Thus $\alpha_{th.exp}$ (P) and $\alpha_{th.exp}$ (T) are differently sensitive to the Sr and X ions in SrX (X = O, S, Se, and Te) lattice is mechanical hard due to bond strengthening and thermal soft due to bond weakening.

We may add that the elastic properties of CaN, SrN, and BaN compounds within the generalized gradient approximation are performed. The bulk and shear moduli, Young's moduli, Poisson's ratio, and brittle/ductile behavior for CaN, SrN, and BaN. The estimated anisotropy parameter, A, shows that SrN has higher degree of elastic isotropy in comparison to CaN and BaN [65]. Furthermore, the density functional theory has been used to compute the structural, electronic, and magnetic properties of Co2CrGe. The total energy calculations lead to stable magnetic configuration and the optimized lattice constant for Heusler alloys [66].

Conclusion

The present study thus addresses, the high-pressure and high-temperature-dependent structural, elastic, and thermodynamical studies in rock salt and cesium chloride structure of SrX (X = O, S, Se, and Te). We have formulated an interatomic pair wise potential that incorporates the long-range Coulomb with charge transfer interactions,

covalent nature of bonds, zero point energy effects and the short-range interactions as charge dipole–dipole and charge dipole-quadruple (van der Waals), as well overlap repulsive interaction up to second-neighbor ions.

From the knowledge of Gibbs's free energies in rock salt and CsCl structure, we determine the pressure induced first-order structural phase transition about 35.5 (SrO), 17.6 (SrS), 14.9 (SrSe), 11.9 (SrTe) GPa. As a next step we determine the cohesive energy as −33.93 (SrO), −60.70 (SrS), −61.43 (SrSe), and −67.26 (SrTe) eV and the volume collapse is about 13.0 (SrO), 11.4 (SrS), 10.7 (SrSe), and 11.1 (SrTe) %. Compressions in SrX (X = O, S Se, Te) at higher pressure indicates the mechanical stiffening of lattice. The phase-transition pressure and volume collapse are consistent with earlier observations. We emphasize that agreement with experimental and theoretical data is not fortuitous, but it is attributed to proper parameterization and formulation of potential with non-central many-body forces in terms of the screening of the effective Coulomb potential through modified ionic charge.

Furthermore, we make effort to determine the second-order aggregate elastic constants C_{ij} under applied pressure and temperature with respect to finite strain. Once pressure and temperature dependence of C_{ij} is known, Cauchy discrepancy and elastic anisotropy in second-order elastic constants, melting temperature, third-order elastic constants C_{ijk}, Cauchy discrepancy and anisotropy in third-order elastic constants, isotropic shear modulii as G_H, G_V, and G_R, Young's modulus E, Poisson's ratio ν, Pugh's ratio ϕ and Vicker's hardness H_V to discuss ductile/brittle nature and mechanical stiffening/thermal softening of SrX lattice. In continuity, Lamé's constant (λ, μ), longitudinal (shear) wave velocity to enumerate the compressibility and shear stiffness of the material, Grüneisen constant, Debye temperature, isothermal compressibility, heat capacity and thermal expansion coefficient to shed light on anharmonicity of SrX (X = O, S, Se, Te). We comment that incorporation of charge transfer interactions, covalent contribution and quantum effects leads to nonzero value of Cauchy discrepancy ($C_{12}-C_{44} \neq 0$) and is a corner stone of the proposed interatomic potential.

From the present investigations on SrX (X = O, S, Se, and Te) we draw the following conclusions:

(a) The volume collapse (V_P/V_0) in terms of compressions in SrX (X = O, S, Se, and Te) at higher pressure indicates the mechanical stiffenening of lattice. The expansion of SrX (X = O, S, Se, and Te) lattice is inferred from steep increase in V_T/V_0 and is attributed to thermal softening of SrX (X = O, S, Se, and Te) lattice.

(b) Larger deviation in Cauchy discrepancy Δ_1^2 emphasizes the importance of the many-body non-central (charge transfer and covalency) interaction and substantial anharmonic effects at high pressures.

(c) Melting temperature (T_M), Vicker's hardness (H_V), shear modulus (G_H), Young's modulus (E) and bulk modulus (B_T) increases with enhanced pressure infers the hardening or stiffening of the lattice and suppressed T_M, G_H, E and B_T variations in temperature suggests the weakening of the lattice as a result of thermal softening of SrX (X = O, S, Se, and Te) lattice.

(d) From the Pugh's ratio (ϕ) we classify SrO as ductile but SrS, SrSe, SrTe are brittle material while to that Poisson's ratio suggest SrX (X = O, S, Se, and Te) its brittle nature. Hence, we conclude that SrS, SrSe, SrTe are brittle in nature at zero pressure the two empirical rules only differ on the exact border between the two types of behavior and SrO is a borderline case between the classes of ductile and brittle materials.

(e) Grüneisen parameter (γ_G) Debye temperature (θ_D), isothermal compressibility (β), heat capacity at constant volume (C_v) and thermal expansion coefficient ($\alpha_{th.\ exp}$) probes the importance of anharmonicity in SrX (X = O, S, Se, Te) at high pressures and temperatures.

(f) Elastic properties showed $T_M(P) > T_M$ (T), $H_V(P) > H_V$ (T), E $(P) > E$ (T), $\theta_D(P) > \theta_D(T)$ and $\alpha_{th.exp}$ $(P) < \alpha_{th.exp}$ (T) Infers that these are differently sensitive to the Sr and X ions as SrX lattice is mechanical hard due to bond strengthening and thermal soft due to bond weakening.

To an end, an interatomic pair wise potential for cubic SrX incorporating the non-central many-body forces as long-range Coulomb with charge transfer interactions, covalent nature of bonds (due to Sr–Sr, Sr–X, and X–X interacting electric fields), quantum effects, charge dipole–dipole and charge dipole-quadruple (van der Waals), and the short-range interactions as overlap repulsion up to second-neighbor ions successfully explains the pressure and temperature induced structural, elastic and thermodynamical properties of SrX (X = O, S, Se, Te) consistent with available results.

Appendix

The expressions for the second order elastic constants for rock salt structure crystals follows:

$$C_{11} = \frac{e^2}{4a^4}\left\{-5.112Z_{\mathrm{m}}^2 + A_1 + \frac{A_2 + B_2}{2} + 9.3204Z(af'(r))\right\} \tag{49}$$

$$C_{12} = \frac{e^2}{4a^4}\left\{0.226Z_{\mathrm{m}}^2 - B_1 + \frac{A_2 - 5B_2}{4} + 9.3204Z(af'(r))\right\} \tag{50}$$

$$C_{44} = \frac{e^2}{4a^4}\left\{2.556Z_{\mathrm{m}}^2 + B_1 + \frac{A_2 + 3B_2}{4}\right\} \tag{51}$$

and

$$B_1 + B_2 = -1.165Z_{\mathrm{m}}^2. \tag{52}$$

Thus second order elastic constants difference lead to finite value at Cauchy pressure:

$$C_{12} - C_{44} \neq 0 \tag{53}$$

Henceforth, polarizability of the ions has effect on the elastic constants. It should be noted that if charge transfer mechanism is not taken in to account, Cauchy relation: $C_{12} - C_{44} = 0$, The Cauchy violations ($C_{12} \neq C_{44}$) is seen by several crystals due to anisotropy in the electron distribution or angle bending. Here, C_{11} represents a measure of resistance to deformation by applied stress and C_{44} represents the measure of resistance to deformation with respect to applied shearing stress. The elastic constants C_{12} and C_{44} are related to the elasticity in shape, which is a shear constant.

The pressure derivatives of second order elastic constants under hydrostatic pressure P are obtained in the form

$$3\Omega\frac{\mathrm{d}B_{\mathrm{T}}}{\mathrm{d}p} = -\left\{13.980Z_{\mathrm{m}}^2 + C_1 - 3A_1 + C_2 - 3A_2 - 167.7648Z(af'(r)) + 41.9420Z\left(a^2f''(r)\right)\right\} \tag{54}$$

$$2\Omega\frac{\mathrm{d}\sigma}{\mathrm{d}p} = -\left\{23.682Z_{\mathrm{m}}^2 + C_1 + \frac{C_2 + 6A_2 - 6B_2}{4} - 50.0752Z(af'(r)) + 13.9808Z\left(a^2f''(r)\right)\right\} \tag{55}$$

$$\Omega\frac{\mathrm{d}C_{44}}{\mathrm{d}p} = -\left\{-11.389Z_{\mathrm{m}}^2 + A_1 - 3B_1 + \frac{C_2 + 2A_2 - 10B_2}{4} + 44.6528Z(af'(r))\right\}. \tag{56}$$

The notation Ω is

$$\Omega = -2.330Z_{\mathrm{m}}^2 + A_1 + A_2 + 27.9612Z(af'(r)). \tag{57}$$

Finally, the third order elastic constants for rock salt structure crystal follows:

$$C_{111} = \frac{e^2}{4a^4}\left\{37.556Z_{\mathrm{m}}^2 + C_1 - 3A_1 - \frac{3A_2 + 9B_2 - C_2}{4} - 89.305Z(af'(r)) + 13.980Z\left(a^2f''(r)\right)\right\} \tag{58}$$

$$C_{112} = \frac{e^2}{4a^4}\left\{-4.836Z_{\mathrm{m}}^2 - \frac{3A_2 + 3B_2 - C_2}{8} - 18.640Z(af'(r)) + 4.66Z\left(a^2f''(r)\right)\right\} \tag{59}$$

$$C_{123} = \frac{e^2}{4a^4}\left\{2.717Z_{\mathrm{m}}^2 + 16.692Z(af'(r))\right\} \tag{60}$$

$$C_{144} = \frac{e^2}{4a^4}\left\{2.717Z_{\mathrm{m}}^2 + 5.564Z(af'(r))\right\} \tag{61}$$

$$C_{166} = \frac{e^2}{4a^4}\left\{-4.836Z_{\mathrm{m}}^2 - 2(B_1 + B_2) - \frac{3A_2 - 3B_2 - C_2}{8} + 5.564Z(af'(r))\right\} \tag{62}$$

$$C_{456} = \frac{e^2}{4a^4}\left\{2.717Z_{\mathrm{m}}^2 - (B_1 + B_2)\right\}. \tag{63}$$

In view of equilibrium condition, the third order elastic constants difference also lead to finite value at Cauchy pressure inferring that polarizability of the ions has effect on the elastic constants:

$$C_{112} - C_{166} \neq 0 \tag{64}$$

$$C_{123} - C_{456} \neq 0 \tag{65}$$

$$C_{144} - C_{456} \neq 0 \tag{66}$$

$$C_{123} - C_{144} \neq 0. \tag{67}$$

Furthermore, the third order elastic constants satisfy the identity:

$$C_{123} + 2C_{456} - 3C_{144} = 0. \tag{68}$$

Various symbols appear in the above expressions are associated with the crystal energy and have the following form in rock salt structure

$$A_1 = \frac{8a^3}{e^2}\left[\frac{\mathrm{d}^2}{\mathrm{d}r^2}V_{ij}(r)\right]_{r=a}, \tag{69}$$

$$A_2 = \frac{16a^3}{e^2}\left[\frac{\mathrm{d}^2}{\mathrm{d}r^2}V_{ii}(r) + \frac{\mathrm{d}^2}{\mathrm{d}r^2}V_{jj}(r)\right]_{r=\sqrt{2}a}, \tag{70}$$

$$B_1 = \frac{8a^3}{e^2}\left[\frac{1}{r}\frac{\mathrm{d}}{\mathrm{d}r}V_{ij}(r)\right]_{r=a}, \tag{71}$$

$$B_2 = \frac{16a^3}{e^2}\left[\frac{1}{r}\frac{\mathrm{d}}{\mathrm{d}r}V_{ii}(r) + \frac{1}{r}\frac{\mathrm{d}}{\mathrm{d}r}V_{jj}(r)\right]_{r=\sqrt{2}a}, \tag{72}$$

$$C_1 = \frac{8a^3}{e^2}\left[r\frac{d^3}{dr^3}V_{ij}(r)\right]_{r=a}, \tag{73}$$

$$C_2 = \frac{16a^3}{e^2}\left[r\frac{d^3}{dr^3}V_{ii}(r) + \frac{d^3}{dr^3}V_{jj}(r)\right]_{r=\sqrt{2}a}. \tag{74}$$

Similarly for CsCl structure crystal, one determines the expressions for the elastic constants. It follows

$$C_{11} = \frac{e^2}{4a^4}\left\{0.7010Z_m^2 + \frac{A_1+2B_1}{6} + \frac{A_2}{2} + 3.1336Z(af'(r))\right\} \tag{75}$$

$$C_{12} = \frac{e^2}{4a^4}\left\{-0.5201Z_m^2 + \frac{A_1-B_1}{6} + 3.1336Z(af'(r))\right\} \tag{76}$$

$$C_{44} = \frac{e^2}{4a^4}\left\{-0.3505Z_m^2 + \frac{A_1+2B_1}{6} + \frac{B_2}{2}\right\} \tag{77}$$

and

$$B_1 + B_2 = -0.3392Z_m^2. \tag{78}$$

The pressure derivatives of second order elastic constants under hydrostatic pressure P take the parametric form

$$3\Omega\frac{dB_T}{dp} = -\Big\{2.0350Z_m^2 + \frac{C_1-3A_1+C_2-3A_2}{18} + 24.4242Z\big(a^2f''(r)\big) - 56.4091Z(af'(r))\Big\} \tag{79}$$

$$2\Omega\frac{d\sigma}{dp} = -\left\{-5.2229Z_m^2 + A_1 - B_1 + \frac{C_2}{2} + 47.9383Z(af'(r))\right\} \tag{80}$$

$$\Omega\frac{dC_{44}}{dp} = -\Big\{1.2321Z_m^2 + \frac{A_1-7B_1+C_1+3A_2-9B_2}{18} + 2.7138Z\big(a^2f''(r)\big) - 6.5791Z(af'(r))\Big\} \tag{81}$$

and Ω is

$$\Omega = -0.3392Z_m^2 + \frac{A_1+A_2}{2} + 9.4008Z(af'(r)) \tag{82}$$

Finally the expressions for the third order elastic constants of CsCl type crystals are

$$C_{111} = \frac{e^2}{4a^4}\Big\{-4.5656Z_m^2 + \frac{C_1-3A_1-24B_1}{18} + \frac{C_2-3A_2}{2} + 13.1567Z(af'(r)) + 2.7138Z\big(a^2f''(r)\big)\Big\} \tag{83}$$

$$C_{112} = \frac{e^2}{4a^4}\Big\{0.7001Z_m^2 + \frac{C_1-3A_1+3B_1}{18} + 6.2677Z(af'(r)) + 2.7138Z\big(a^2f''(r)\big)\Big\} \tag{84}$$

$$C_{123} = \frac{e^2}{4a^4}\Big\{1.2000Z_m^2 + \frac{C_1-3A_1+3B_1}{18} - 15.9799Z(af'(r)) + 2.7138Z\big(a^2f''(r)\big)\Big\} \tag{85}$$

$$C_{144} = \frac{e^2}{4a^4}\Big\{1.2000Z_m^2 + \frac{C_1-3A_1+3B_1}{18} - 5.3266Z(af'(r)) + 0.9046Z\big(a^2f''(r)\big)\Big\} \tag{86}$$

$$C_{166} = \frac{e^2}{4a^4}\Big\{0.3609Z_m^2 + \frac{C_1-3A_1+3B_1}{18} - (B_1+B_2) - 5.3266Z(af'(r)) + 0.9046Z\big(a^2f''(r)\big)\Big\} \tag{87}$$

$$C_{456} = \frac{e^2}{4a^4}\left\{1.2000Z_m^2 + \frac{C_1-3A_1+3B_1}{18}\right\} \tag{88}$$

Here, we define following form in CsCl structure

$$A_1 = \frac{16a^3}{e^2}\left[\frac{d^2}{dr^2}V_{ij}(r)\right]_{r=a\sqrt{3}}, \tag{89}$$

$$A_2 = \frac{8a^3}{e^2}\left[\frac{d^2}{dr^2}V_{ii}(r) + \frac{d^2}{dr^2}V_{jj}(r)\right]_{r=2a}, \tag{90}$$

$$B_1 = \frac{16a^3}{e^2}\left[\frac{1}{r}\frac{d}{dr}V_{ij}(r)\right]_{r=a\sqrt{3}}, \tag{91}$$

$$B_2 = \frac{8a^3}{e^2}\left[\frac{1}{r}\frac{d}{dr}V_{ii}(r) + \frac{1}{r}\frac{d}{dr}V_{jj}(r)\right]_{r=2a} \tag{92}$$

$$C_1 = \frac{16a^3}{e^2}\left[r\frac{\partial^3}{\partial r^3}V_{ij}(r)\right]_{r=a\sqrt{3}} \tag{93}$$

and

$$C_2 = \frac{8a^3}{e^2}\left[r\frac{d^3}{dr^3}V_{ii}(r) + r\frac{d^3}{dr^3}V_{jj}(r)\right]_{r=2a} \tag{94}$$

in terms of the short-range energy

$$V_{ij}(r) = \sum_{ij} b\beta_{ij}\exp\left(\frac{r_i + r_j - r_{ij}}{\rho}\right) - \sum_{ij}\frac{C}{r_{ij}^6} - \sum_{ij}\frac{D}{r_{ij}^8}. \tag{95}$$

The short-range interaction (SR) energy is expressed in terms of the overlap repulsion (first term) and the vdW $d-d$ and $d-q$ attractions (second and third terms), respectively.

References

1. Potzel, O., Taubmann, G.: The pressure induced B1–B2 phase transition of alkaline halides and alkaline earth chalcogenides. A first principles investigation. J. Solid State Chem. **184**, 1079 (2011)
2. Souadkia, M., Bennecer, B., Kalarasse, F., Mellouki, A.: Ab initio calculation of vibrational and thermodynamic properties of SrX (S, Se, Te) in the B1 (NaCl) and B2 (CsCl) structures. Comput. Mater. Sci. **50**, 1701 (2011)
3. Luo, H., Greene, R.G., Ruoff, A.L.: High-pressure phase transformation and the equation of state of SrSe. Phys. Rev. B **49**, 15341 (1994)
4. Sato, Y., Jeanloz, R.: Phase Transition in SrO. J. Geophys. Res. Solid Earth **86**, 11773 (1981)
5. Zimmer, H.G., Winzen, H., Sayassen, K.: High-pressure phase transitions in CaTe and SrTe. Phys. Rev. B **32**, 4066 (1985)
6. Son, P.R., Bartels, R.A.: CaO and SrO single crystal elastic constants and their pressure derivatives. J. Phys. Chem. Solids **33**, 819 (1972)
7. Syassen, K.: Pressure induced structural transition in SrS. Phys. Status Solidi A **91**, 11 (1985)
8. Khenata, R., Baltache, H., Rerat, M., Driz, M., Sahnoun, M., Bouhafs, B., Abbar, B.: First-principle study of structural, electronic and elastic properties of SrS, SrSe and SrTe under pressure. Phys. B **339**, 208 (2003)
9. Habas, M.P., Dovesi, R., Lichanot, A.: The phase transition in alkaline-earth oxides: a comparison of ab initio Hartree-Fock and density functional calculations. J. Phys. Condens. Matter **10**, 6897 (1998)
10. Yan, C., Lai-Yu, L., Ou-He, J., Xiang-Rong, C.: Phase transition and thermodynamic properties of SrS via first-principles calculations. Chin. Phys. B **17**, 1355 (2008)
11. Kholiya, K., Gupta, B.R.K.: Theoretical investigation of phase transition properties in strontium chalcogenides using potential model. Phase Transitions **81**, 403 (2008)
12. Tsuchiya, T., Kawamura, K.: Systematics of elasticity: ab initio study in B1-type alkaline earth oxides. J. Chem. Phys. **114**, 10086 (2001)
13. Born, M., Huang, K.: Dynamical theory of crystal lattices. Clarendon, Oxford (1956)
14. Vashishta, P., Kalia, R.K., Nakano, A.: Interaction potential for silicon carbide: a molecular dynamics study of elastic constants and vibrational density of states for crystalline and amorphous silicon carbide. J. Appl. Phys. **101**, 103515 (2007)
15. Stillinger, F.H., Weber, T.A.: Computer simulation of local order in condensed phases of silicon. Phys. Rev. B **31**, 5262 (1985)
16. Motida, K.: Szigeti charge and its correlation with hyperfine coupling constant of doped Mn^{2+} ion in divalent metal compounds. J. Phys. Soc. Jpn. **49**, 213 (1980)
17. Motida, K.: Effect of covalency on phonon dispersion relations in NaCl type alkali halide crystal. J. Phys. Soc. Jpn. **55**, 1636 (1986)
18. Slater, J.C., Kirkwood, J.G.: The vander Waals forces in gases. Phys. Rev. **37**, 682 (1931)
19. Tosi, M.P.: Cohesion of ionic solids in the born model. Solid State Phys. **16**, 1 (1964)
20. Hafemeister, D.W., Flygare, W.H.: Outer-shell overlap integral as a function of distance for halogen–halogen, halogen–alkali, and alkali–alkali ions in the alkali halide lattices. J. Chem. Phys. Soc. **43**, 795 (1965)
21. Lowdin, P.O.: Quantum theory of cohesive properties of solids. Adv. Phys. **5**, 1 (1956)
22. Lundqvist, S.O.: Three body potential for alkali halides. Ark. Fys. **12**, 263 (1957)
23. Varshney, D., Shriya, S.: Elastic, mechanical and thermodynamic properties at high pressures and temperatures of transition metal monocarbides. Int. J. Refract. Metals Hard Mater **41**, 375 (2013)
24. Singh, R.K.: Many body interactions in binary ionic solids. Phys. Rep. **85**, 259 (1982)
25. Varshney, D., Sharma, P., Kaurav, N., Shah, S., Singh, R.K.: Study of elastic properties and their pressure dependence of semi magnetic semiconductors. J. Phys. Soc. **74**, 382 (2005)
26. Varshney, D., Joshi, G., Kaurav, N., Singh, R.K.: Structural phase transition (zincblende–rocksalt) and elastic properties in AlY (Y = N, P and As) compounds: pressure-induced effects. J. Phys. Chem. Solids **70**, 451 (2009)
27. Varshney, D., Joshi, G., Varshney, M., Shriya, S.: Pressure induced structural phase transition and elastic properties in BSb, AlSb, GaSb and InSb compounds. Phys. B Condens. Matter **405**, 1663 (2010)
28. Varshney, D., Joshi, G., Varshney, M., Shriya, S.: Pressure dependent elastic and structural (B3–B1) properties of Ga based monopnictides. J. Alloys Compd. **495**, 23 (2010)
29. Varshney, D., Joshi, G.: High-pressure structural phase transition and elastic properties of Ga1-x InxAs semiconducting compounds. Eur. Phys. J. B **70**, 523 (2009)
30. Varshney, D., Kaurav, N., Kinge, R., Singh, R.K.: High-pressure structural (B1–B2) phase transition and elastic properties of II–VI semiconducting Sr chalcogens. Comput. Mater. Sci. **41**, 529 (2008)
31. Varshney, D., Shriya, S., Varshney, M., Singh, N., Khenata, R.: Elastic and thermodynamical properties of cubic (3C) silicon carbide under high pressure and high temperature. J. Theor. Appl. Phys. **9**, 221–249 (2015)
32. Varshney, D., Joshi, G., Varshney, M., Shriya, S.: Pressure induced mechanical properties of boron-based pnictides. Solid State Sci. **12**, 864 (2010)
33. Varshney, D., Kaurav, N., Kinge, R., Singh, R.K.: Pressure induced phase transition (B1–B2) and elastic properties in alkaline earth BaX (X = S, Se and Te) chalcogenides. Phase Transitions **81**, 1 (2008)
34. Varshney, D., Kaurav, N., Kinge, R., Singh, R.K.: High-pressure induced structural phase transition in alkaline earth CaX (X = S, Se and Te) semiconductors: NaCl-type (B1) to CsCl-type (B2). J. Alloys Compd. **484**, 239 (2009)
35. Varshney, D., Kaurav, N., Kinge, R., Singh, R.K.: Pressure induced phase transition and elastic properties of Y and Sc antimonides. J. Alloys Compd. **448**, 250 (2008)
36. Varshney, D., Singh, N.: Thermoelectric power of metallic Rb3C60: phonon-drag and carrier diffusion contributions. J. Theor. Appl. Phys. **6**(37), 1–9 (2012)
37. Varshney, D., Dodiya, N.: Metallic and semi-conducting resistivity behavior of $La_{0.7}Ca_{0.3-x}$ K_xMnO_3 (x = 0.05, 0.1) manganites. J. Theor. Appl. Phys. **9**, 45–48 (2015)
38. Tessman, J.R., Kahn, A.H., Shockley, W.: Electronic polarizabilities of ion in crystals. Phys. Rev. **92**, 890 (1953)
39. Shannon, R.D.: Dielectric polarizabilities of ions in oxides and fluorides. J. Appl. Phys. **73**, 348 (1993)
40. Weast, R.C. (ed.): Handbook of chemistry and physics, 63rd edn. CRC, Boca Raton (1982)
41. Murnaghan, F.D.: The compressibility of media under extreme pressures. Proc. Natl. Acad. Sci. **3**, 244 (1944)
42. Goel, P., Choudhury, N., Chaplot, S.L.: Superionic behavior of lithium oxide Li2O: a lattice dynamics and molecular dynamics study. Phys. Rev. B **70**, 174307 (2004)

43. Li, X.-F., Chen, X.-R., Meng, C.-M., Ji, G.-F.: Ab initio calculations of elastic constants and thermodynamic properties of Li_2O for high temperatures and pressures. Solid State Commun. **139**, 197 (2006)
44. Yun-Dong, G., Ze-Jin, Y., Qing-He, G., Zi-Jiang, L., Wei, D.J.: The phase transition, and elastic and thermodynamic properties of CaS derived from first-principles calculations. Phys. Condens. Matter **20**, 115203 (2008)
45. Vukcevich, M.R.: The elastic constants of cubic crystals with covalent and partially covalent bonds. Phys. Stat. Solidi (b) **54**, 435 (1972)
46. Barsch, G.R.: Relation between third-order elastic constants of single crystals and polycrystals. J. Appl. Phys. **39**, 3780 (1968)
47. Hill, R.: The elastic behaviour of a crystalline aggregate. Proc. Phys. Soc. (London) **65A**, 349 (1952)
48. Voigt, W.: Lehrbuch der Kristallphysik. Teubner, Leipzig (1928)
49. Reuss, A.: Calculation of the flow limits of mixed crystals on the basis of the plasticity of monocrystals. Angew Z. Math. Mech. **9**, 49 (1929)
50. Pugh, S.F.: Relations between the elastic moduli and the plastic properties of polycrystalline pure metals. Phil. Mag. **45**, 823 (1954)
51. Frantsevich, N., Voronov, F.F., Bokuta, S.A.: In: Frantsevich, I.N. (eds.) Elastic constants and elastic moduli of metals and insulators handbook. Naukova Dumka, Kiev, p. 60 (1983)
52. Schreiber, E., Anderson, O.L., Soga, N.: Elastic constants and their measurements. McGraw-Hill, New York (1973)
53. Harrison, W.A.: Electronic structure and properties of solids. Dover, New York (1989)
54. Bouhemadou, A., Khenata, R., Kharoubi, M., Seddik, T., Reshak, A.H., Al-Douri, Y.: FP-APW+ lo calculations of the elastic properties in zinc-blende III-P compounds under pressure effects. Comput. Mater. Sci. **45**, 474 (2009)
55. Maachou, A., Aboura, H., Amrani, B., Khenata, R., Bin Omran, S., Varshney, D.: Structural stabilities, elastic and thermodynamic properties of Scandium Chalcogenides via first-principles calculations. Comput. Mater. Sci. **50**, 3123 (2011)
56. Kleinman, L.: Deformation potentials in silicon. Phys. Rev. **128**, 2614 (1962)
57. Blackman, M.: The specific heat of solids. Proc. R. Soc. Lond. A **181**, 58 (1942)
58. Blackman, M.: The specific heat of solids. Proc. R. Soc. Lond. A **159**, 416 (1937)
59. Blackman, M.: The specific heat of solids. Proc. R. Soc. Lond. A **149**, 126 (1935)
60. Blackman, M.: The specific heat of solids. Proc. R. Soc. Lond. A **148**, 384 (1935)
61. Blackman, M.: The specific heat of solids. Proc. R. Soc. Lond. A **148**, 365 (1935)
62. Gopal, E.S.R.: Specific heats at low temperatures. Plenum Press, New York (1966)
63. Tari, A.: The specific heat of matter at low temperatures. Imperial College Press, London (2003)
64. Souadkia, M., Bennecer, B., Kalarasse, F.: Ab initio lattice dynamics and thermodynamic properties of SrO under pressure. J. Phys. Chem. Solids **73**, 129 (2012)
65. Sharifzadeh, H.S., Sharifzadeh, S.S., Kanjouri, F., Esmailian, A.: Mechanical properties of CaN, SrN, and BaN compounds by density functional theory. J. Theor. Appl. Phys. **7**(16), 1–5 (2013)
66. Rai, D.P., Shankar, A., Sandeep, Ghimire, M.P., Thapa, R.K.: Electronic and magnetic properties of a full-Heusler alloy Co_2-CrGe: a first-principles study. J. Theor. Appl. Phys. **7**(3), 1–6 (2013)